Vol. 19, Sup. 1 (2020) 495-520
Revista Mexicana de Ingeniería Química

# Average velocity profile between a fluid layer and a porous medium: Brinkman boundary layer

# Perfil de velocidad promedio entre una capa de fluido y un medio poroso: La capa límite de Brinkman

R. Hernandez-Rodriguez[1], B. Goyeau[2], P. Angot[3] and J. A. Ochoa-Tapia[2*]

[1]*División de Ciencias Básicas e Ingeniería, Universidad Autónoma Metropolitana-Iztapalapa. Av. San Rafael Atlixco 186, col. Vicentina, 09340 Mexico, Mexico..*
[2]*Laboratoire EM2C, UPR-CNRS 288, Ecole Centrale-Supélec, Université Paris-Saclay, Grande Voie des Vignes F92-295 Châtenay-Malabry Cedex, France.*
[3]*Aix-Marseille Université, Institut de Mathématiques de Marseille, UMR-CNRS 7373, Centrale Marseille, 39 rue F. Joliot-Curie, 13453 Marseille cedex 13, France.*

Received: September 8, 2019; Accepted: April 23, 2020

**Abstract**

It has been mentioned that, the existence of some terms in Darcy's law are the result of the up-scaling method applied to the Stokes flow problem at the pore-scale. To address this debate, in this work we perform, at the pore-scale, flow simulations in a free fluid/porous medium system using different models of granular porous media. The local velocity obtained from the Stokes equation allows to obtain the Darcy-scale velocity profiles by a direct averaging instead of using the up-scaled model. The results show the existence of a smooth transition zone in the average velocity profiles near the free fluid/porous medium inter-region. The size and shape of such transition zone depend on the size of the averaging domain and they are a result of averaging local quantities and not a result of solving average equations. In this way, we confirm the existence of an average velocity boundary layer (*i.e.* Brinkman boundary layer); thus the pertinence of considering other terms in Darcy's law can be certainly justified. We have also determined the extension of the influence of the flow in the free fluid inside the porous medium and the perturbation of the flow in porous medium on the flow in the free fluid.

*Keywords*: average velocity, boundary layer, pore-scale simulations, Stokes flow.

**Resumen**

Se dice que la existencia de algunos términos en la ley de Darcy son resultado del método de escalamiento aplicado al problema de flujo de Stokes a la escala de poro. En este trabajo, para tratar de aclarar esta situación, hemos realizado simulaciones del flujo a la escala de poro, en un sistema fluido libre-medio poroso usando diferentes modelos de medio poroso con partículas. La velocidad local obtenida permitió la obtención del perfil de velocidad promedio a la escala de Darcy a través del promediado directo y no de la solución de un modelo promedio. Los resultados muestran la existencia de una zona de transición en los perfiles de velocidad promedio en la cercanía de la inter-región medio poroso/fluido libre. El tamaño y forma de tal zona depende de la dimensión del dominio de promediado. Esto es el resultado de promediar cantidades locales y no de la solución de ecuaciones promedio. De esta manera, se confirma la existencia de una capa límite (capa límite de Brinkman) y por ello puede ser pertinente el considerar otros términos en la ley de Darcy. También, se el alcance del efecto del flujo en el fluido libre sobre el medio poroso y la perturbación provocada por el medio poroso en el flujo del fluido libre.

*Palabras clave*: velocidad promedio, capa límite, simulaciones a la escala de poro, flujo de Stokes.

* *Corresponding author. E-mail*: jaot@xanum.uam.mx
*Tel. +(52)-55-58-04-46-49*
https://doi.org/10.24275/rmiq/Fen843
*issn-e*: 2395-8472

# 1 Introduction

There are many chemical engineering operations or processes that use porous materials, in order to increase the volumetric surface area to separate or transform chemical species that are carried by the surrounding fluid (Bird et al., 2002; Froment et al., 2010; Seader et al., 2016). In this way, in the process design, the modeling of the transport between fluids and porous media must be considered. Under many operation conditions the convective transport can not be neglected, as a consequence the velocity distribution in a fluid/porous medium inter-region is required. Similar situations can be also found in many natural processes, for example, cellular scaffolds (Yu, 2012), canopy flow (Clark et al., 2007; Macdonald, 2000; Shavit et al., 2009), benthic boundary layers (Boudreau and Jorgensen, 2001; Jørgensen, 2001), forest fire modeling (Margerit and Séro-Guillaume, 2002; Séro-Guillaume and Margerit, 2002), and many others.

For incompressible flow of a Newtonian fluid in and around a porous medium, when the motion is slow enough, the local velocity of a fluid is governed by the Stokes and the continuity equations. These must be solved subject to the non-slip boundary condition at the solid-fluid interfaces along with certain boundary conditions at the entrances and exits of the system. However, due to the disparity of characteristic length-scales and the complex geometry of a porous medium, the solution of the pore-scale model is a tremendous computational challenge. For such reason, a more convenient approach is to model the fluid flow in terms of average equations. In this sense, it is generally accepted that the flow in the bulk of a porous medium ($\omega-$region) is governed by the Darcy's law, which in vector form can be written as

$$\left\langle \mathbf{v}_\beta \right\rangle_\omega = -\frac{\mathbf{K}_{\beta\omega}}{\mu_\beta} \cdot \left( \nabla \left\langle p_\beta \right\rangle_\omega^\beta - \rho_\beta \mathbf{g} \right) \tag{1}$$

where $\mathbf{K}_{\beta\omega}$ is the permeability tensor of the bulk of the porous medium, $\langle \mathbf{v}_\beta \rangle_\omega$ is the superficial average velocity (also known as the filtration velocity or the Darcy's velocity) and $\langle p_\beta \rangle_\omega^\beta$ is the intrinsic average pressure. These two kind of average quantities are defined in terms of the integration of their pore-scale counterpart in the fluid domain $\mathscr{V}_\beta$ contained within an averaging domain $\mathscr{V}$ (*i.e.*, representative elementary volume or REV) by

$$\langle \varphi \rangle |_{\mathbf{x}} = \frac{1}{V} \int\limits_{\mathbf{r} \in \mathscr{V}_\beta(\mathbf{x})} \varphi|_{\mathbf{r}} dV \quad \text{where} \quad \varphi = p_\beta, \mathbf{v}_\beta \tag{2a}$$

$$\langle \varphi \rangle^\beta |_{\mathbf{x}} = \frac{1}{V_\beta(\mathbf{x})} \int\limits_{\mathbf{r} \in \mathscr{V}_\beta(\mathbf{x})} \varphi|_{\mathbf{r}} dV \tag{2b}$$

which are related by $\langle \varphi \rangle |_{\mathbf{x}} = \varepsilon_\beta(\mathbf{x}) \langle \varphi \rangle^\beta |_{\mathbf{x}}$, where $\varepsilon_\beta(\mathbf{x})$ is the fluid volume fraction that can be position dependent. In eqs. (2), we have used $\mathbf{x}$ and $\mathbf{r}$ to indicate the position vectors that locate the centroid of the averaging volume and of any point in the system, respectively.

Another proposal to describe the fluid velocity in the porous medium is the Darcy-Brinkman equation (Brinkman, 1949a,b), which is given by

$$\mathbf{0} = -\nabla \left\langle p_\beta \right\rangle_\omega^\beta + \rho_\beta \mathbf{g} + \mu_{eff} \nabla^2 \left\langle \mathbf{v}_\beta \right\rangle_\omega - \mu_\beta \mathbf{K}_{\beta\omega}^{-1} \cdot \left\langle \mathbf{v}_\beta \right\rangle_\omega \tag{3}$$

where $\mu_{eff}$ is the effective viscosity of the porous medium. Both Darcy and Darcy-Brinkman equations are results of up-scaling the Stokes flow problem, that require the imposition of several reasonable restrictions. In general, due to the disparity of characteristic length-scales, these equations are only valid in the bulk of the porous medium (Whitaker, 1999). As a consequence, in many cases, the Brinkman correction to Darcy's law is negligible for most of the porous region. However, due to the rapid variations of the fluid volume fraction and velocity at the boundaries of the porous medium, Darcy's law does not necessarily holds near the porous media boundaries (Goharzadeh et al., 2005). For this reason, the Brinkman correction is often kept, which arises the possibility of keeping another contributions of the same order of magnitude (*i.e.*, terms that contain porosity spatial variations) (Whitaker, 1999).

On the other hand, for the aforementioned average model, the fluid velocity in the free fluid ($\eta-$region) is governed by the Stokes equation, where the local pressure and velocity are replaced by their corresponding averages, *i.e.*, $\varphi_\beta \Rightarrow \left\langle \varphi_\beta \right\rangle_\eta^\beta$ (Ochoa-Tapia and Whitaker, 1995a).

$$\mathbf{0} = -\nabla \left\langle p_\beta \right\rangle_\eta^\beta + \rho_\beta \mathbf{g} + \mu_\beta \nabla^2 \left\langle \mathbf{v}_\beta \right\rangle_\eta \tag{4}$$

It should be noted that, we have used the subscripts $\omega$ and $\eta$ to indicate variables or effective coefficients associated to the homogeneous porous medium and clear fluid, respectively.

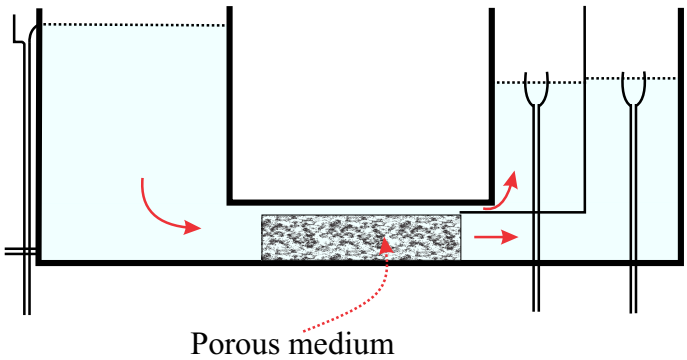


Fig. 1. Schematic view of the experimental setup used by Beavers and Joseph (1967).

The completion of the model given by the Darcy's equation or Darcy-Brinkman equation for the porous medium region and Stokes average equation for the fluid region requires coupling boundary conditions. For the system shown in Fig. 1, Beavers and Joseph (1967) proposed an empirical boundary condition analogous to Newton's cooling law to couple the Darcy's velocity $\langle v_\beta \rangle_\omega$ with the slip velocity of the fluid at the free fluid/porous medium interface $\langle v_\beta \rangle_\eta|_{y=0}$, which is given by

$$\left.\frac{d\langle v_\beta\rangle_\eta}{dy}\right|_{y=0} = \frac{\alpha_{BJ}}{\sqrt{K_{\beta\omega}}}\left(\langle v_\beta\rangle_\eta\Big|_{y=0} - \langle v_\beta\rangle_\omega\right) \tag{5}$$

where $\alpha_{BJ}$ is an empirical slip coefficient. In addition, Beavers and Joseph (1967) set-up an experimental system consisting of a channel partially filled with a porous medium (see Fig. 1). In this way, they determined the fluid flow through the free fluid region and the $\alpha_{BJ}$ coefficient was obtained by fitting their experimental data.

For the case in which Darcy's law is used, several theoretical and experimental works seeking to address the coupling situation have been presented. Many of them have used as a system a channel partially filled with a porous medium. Other studies have focused on the determination of $\alpha_{BJ}$, where it has been found to depend strongly on the microstructure of the boundaries of the porous medium (Beavers et al., 1970; Morad and Khalili, 2009; Richardson, 1971; Taylor, 1971).

In contrast, to couple the Darcy-Brinkman equation with the Stokes average equation, Ochoa-Tapia and Whitaker (1995a), using the volume averaging method, derived a jump boundary condition for the stress. For the system used by Beavers and Joseph (1967), it takes the following form

$$\varepsilon_{\beta\omega}^{-1}\left.\frac{d\langle v_\beta\rangle_\omega}{dy}\right|_{y=0} - \left.\frac{d\langle v_\beta\rangle_\eta}{dy}\right|_{y=0} = \frac{\beta_{OTW}}{\sqrt{K_{\beta\omega}}}\langle v_\beta\rangle_\omega\Big|_{y=0} \tag{6}$$

where $\beta_{OTW}$ is a dimensionless coefficient of the order of one, which was determined by adjusting the experimental data reported by Beavers and Joseph (1967). Several studies have focused on its theoretical determination (Chandesris and Jamet, 2006, 2007; Goyeau et al., 2003; Valdés-Parada et al., 2009). In the derivation of this boundary condition an important step is the use of a generalized transport equation (GTE) for momentum transport, which is similar to the Brinkman equation, with the difference that the effective coefficients are position dependent, the effective viscosity is equal to $\mu_\beta/\varepsilon_\beta(\mathbf{x})$ and considers a second viscous term known as the second Brinkman correction (Ochoa-Tapia and Whitaker, 1995a,b; Valdés-Parada et al., 2007). This GTE has the property that it is continuously reduced from the average form of Stokes equation in the bulk of the free fluid to Darcy's equation in the bulk of the porous medium. In this way, it includes the existence of a transition zone in the average velocity profile in the inter-region between the homogeneous parts of the system. Other works have used a simplified form of GTE to derive boundary conditions and to predict the associated coefficients (Chandesris and Jamet, 2006, 2007; Goyeau et al., 2003; Valdés-Parada et al., 2013, 2009, 2007). The GTE has also been involved in the derivation of boundary conditions for multidimensional flow (Angot et al., 2017). However, in some cases the existence of a transition zone is seen as a consequence of particular average momentum models, and not as a result of averaging the local velocity profile.

Recently, Ochoa-Tapia et al. (2017) addressed this situation by assuming that the porous medium, in a system like Beavers-Joseph's, is consolidated and formed by capillary pores of the same diameter, where the flow occurs in the same direction that the free fluid flow in the upper channel. The laminar flow assumption allowed those authors to obtain analytic expressions for the average velocity profiles everywhere in the system. In this way, they showed the existence of a continuous transition zone between the velocity of the bulk of the porous medium (Darcy's velocity) and the one in the bulk of the fluid region, which include the so called Brinkman boundary layer (Goharzadeh et al., 2005; Morad and Khalili, 2009). However, the geometry used in that work does not allow mass and momentum transfer between the two regions of the system. Therefore, for other type of porous media, the existence of a transition zone in the average velocity profiles near of their boundaries may be questionable. For such reason, in this paper, in order to confirm the existence of a transition zone near the porous medium boundaries as a direct result of averaging local quantities, we extend the work of Ochoa-Tapia et al. (2017) using granular porous media micro-structures, which consist of periodic arrays of horizontal cylinders or prisms perpendicular to the main flow direction. These configurations for the porous media allow mass and momentum transfer between the free fluid and the one in the porous media, thus the conclusions drawn in this work may retain generality. With this in mind, this paper is organized as follows: In Section 2, the free fluid/porous medium system and the micro-scale model that governs the total mass and momentum transfer are presented. Then, the solution method of the micro-scale model in the fluid/porous medium system is described. In this way, the domain of application of Stokes model for the channel system is determined. Finally, in the same section, the specific averaging operators and average velocity profiles from the direct numerical simulation (DNS) solution are presented. In addition, the existence of a transition layer for the average velocity inside the porous medium is confirmed. After that, in Section 3, the local velocity profiles and the determination of the distance of influence of the flow in one homogeneous region on the other is shown. Finally, some discussion and the corresponding conclusions are presented in Sections 5 and 6.

## 2 The Stokes problem in a channel partially filled with a porous medium

### 2.1 *Fluid-porous medium system and local model*

The system under consideration is shown in Fig. 2, which is an schematic view of the system used by Beavers and Joseph (1967) to experimentally determine the effect of the porous medium boundaries on the flow of a fluid flow through the upper gap in the channel. The system consists of a channel partially filled with a homogeneous porous medium made of a rigid solid phase ($\sigma-$phase). The characteristic lengths of both homogeneous regions, $L_\eta$ and $L_\omega$, as well as the corresponding to the sampling volume, $r_0$, are shown in Fig. 2. The same fluid phase that saturates the porous medium flows over it. The fluid region above the porous medium is identified as the $\eta-$region and the region occupied by the porous medium is identified as the $\omega-$region. The flow is assumed to be stationary, incompressible, and slow enough to neglect inertial effects. On the basis of these assumptions, for a Newtonian fluid, the governing equations for mass and momentum transfer are

*Continuity equation*

$$\nabla \cdot \mathbf{v}_\beta = 0 \qquad \text{in the } \beta - \text{phase} \tag{7a}$$

*Stokes equation*

$$\mathbf{0} = -\nabla p_\beta + \rho_\beta \mathbf{g} + \mu_\beta \nabla^2 \mathbf{v}_\beta \qquad \text{in the } \beta - \text{phase} \tag{7b}$$

where $\mathbf{v}_\beta$ is the local velocity, $p_\beta$ is the local pressure, $\mu_\beta$ is the dynamic viscosity, $\rho_\beta$ is the density and $\mathbf{g} = -g\mathbf{j}$ is the gravity vector. Eqs. (7a) and (7b) must be solved subject to the non-slip boundary condition at the solid-fluid interfaces ($\mathscr{A}_{\beta\sigma}$) given by

$$\mathbf{v}_\beta = \mathbf{0} \qquad \text{at} \qquad \mathscr{A}_{\beta\sigma} \tag{7c}$$

This boundary condition also must be satisfied at the surface of the horizontal plates that bound the channel. In addition, to complete the statement of the boundary value problem, it is necessary to provide the boundary conditions at entrances and exits of the system ($\mathscr{A}_{\beta,e}$). In the case here considered, the flow is driven by a fixed pressure drop between the entrance and exit of the channel, which can be expressed by

$$-\frac{\partial p_\beta}{\partial x} = \frac{p_\beta|_{x=0} - p_\beta|_{x=L}}{L} = \text{constant} \qquad \text{for all } y \tag{7d}$$

In Fig. 2, portions (*i.e.*, samples) of the system in different locations are shown: (a) in the bulk of $\eta-$region, (d) in the bulk of the $\omega-$ region, and (b), (c) and (e) in the three inter-regions. Along this work, we will use the term inter-region to identify those zones in which the microstructure of the system undergoes rapid changes and, as a consequence, the volume fraction and other effective coefficients change rapidly.

## 2.2 *Solution of the local model*

In order to solve the local model in the channel system, as a first approximation, we assume that the porous media consist of horizontal cylindrical or prism-shaped particles, whose main axis are perpendicular to the main flow direction. All the calculations are restricted to the arrangements of the unit cells shown in Fig. 3. In this way, due to the fully developed flow assumption, the velocity field is periodic in the $x$ direction, thus it is enough to carry out the solution in a subdomain as the one shown in Fig. 4. As a consequence, the pressure drop is constant in the $x$ direction and the velocity field must satisfy

$$\mathbf{v}_\beta(\mathbf{r}) = \mathbf{v}_\beta(\mathbf{r} + \ell\mathbf{i}) \tag{8}$$

where $\ell$ is the characteristic length of the periodic unit cell and $\mathbf{i}$ the unit vector in the $x$ direction. In addition, to avoid unnecessary calculations, instead of using the non-slip boundary condition at the lower plate of the channel, only a part of the porous medium is considered. This is because far enough inside the porous medium the local velocity profile is periodic in the two directions. In this way, the size $L_\omega$ must be chosen in such way that the symmetry condition can be imposed in the horizontal border of the unit cell.

$$\mathbf{n}_\beta \cdot \nabla\mathbf{v}_\beta = \mathbf{0} \quad \text{at} \quad y = -L_\omega \tag{9}$$

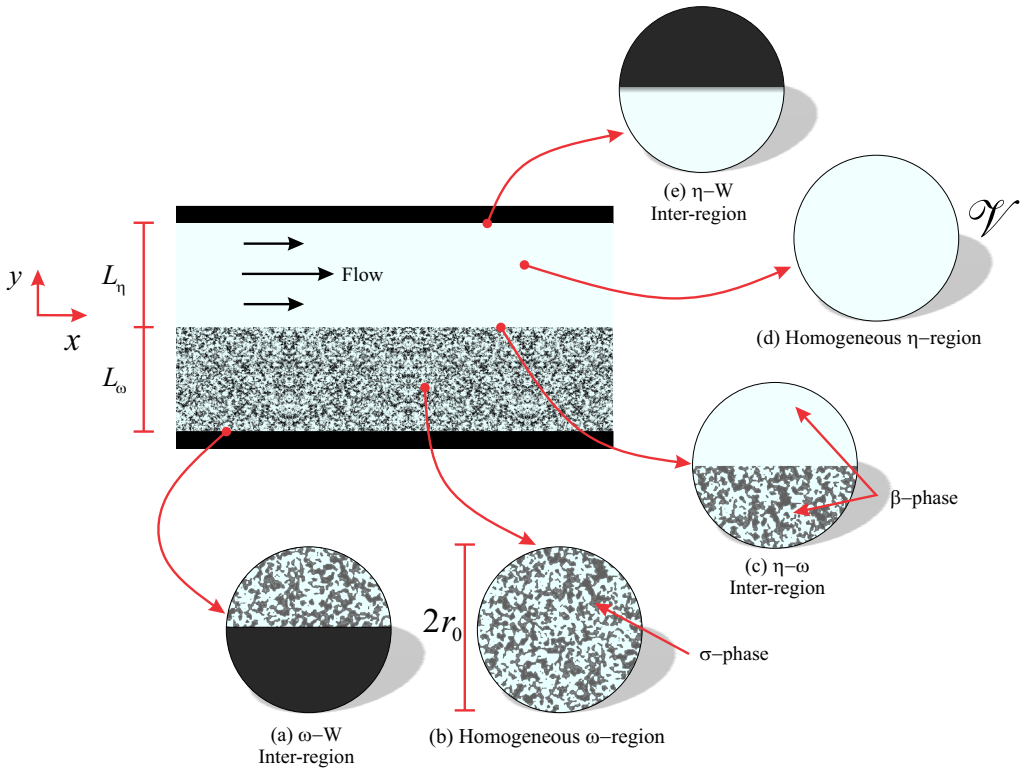


Fig. 2. Close ups of the samples in homogeneous regions and inter-regions of the channel system used by Beavers and Joseph (1967). The characteristic lengths of the homogeneous regions and the sampling volume are $L_\eta$, $L_\omega$, and $r_0$, respectively.

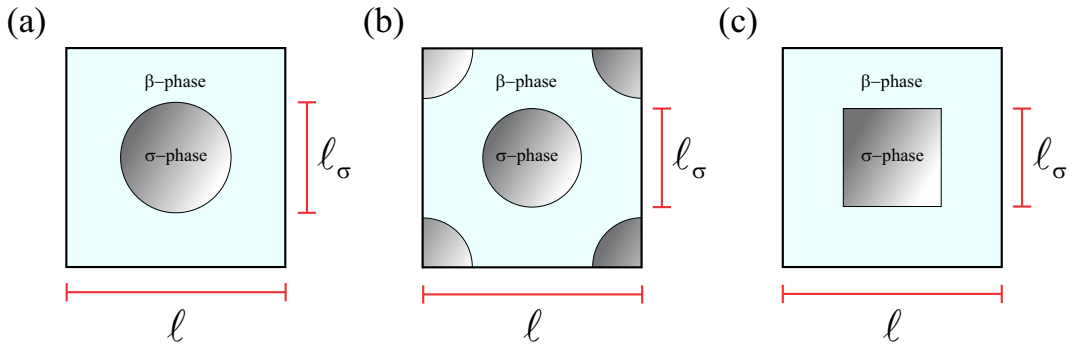


Fig. 3. Cross section of the unit cells for the bulk of the porous medium: (a) cylinders in line, (b) staggered cylinders, and (c) square prisms in line.

Then, for simplicity, we introduce the following dimensionless variables

$$X = \frac{x}{\ell};\quad Y = \frac{y}{\ell};\quad \mathbf{u} = \frac{\mathbf{v}_\beta \ell \rho_\beta}{\mu_\beta};\quad p = \frac{\ell^2 \rho_\beta (p_\beta + \rho_\beta y g)}{\mu_\beta^2} \tag{10}$$

Thus, eqs. (7)-(9) take the form

$$\nabla \cdot \mathbf{u} = 0 \quad \beta - \text{phase} \tag{11a}$$

$$\mathbf{0} = -\nabla p + \nabla^2 \mathbf{u} \quad \beta - \text{phase} \tag{11b}$$

B. C. 1 $$\mathbf{u} = \mathbf{0} \quad \text{at} \quad \mathscr{A}_{\beta\sigma} \tag{11c}$$

B. C. 2 $$\mathbf{u} = \mathbf{0} \quad \text{at} \quad Y = L_\eta/\ell \tag{11d}$$

B. C. 3 $$\mathbf{n}_\beta \cdot (\nabla \mathbf{u}) = \mathbf{0} \quad \text{at} \quad Y = -L_\omega/\ell \tag{11e}$$

$$\mathbf{u}(\mathbf{r}/\ell) = \mathbf{u}(\mathbf{r}/\ell + \mathbf{i}) \tag{11f}$$

$$-\frac{\partial p}{\partial X} = \left(\frac{p_\beta|_{x=0} - p_\beta|_{x=L}}{L}\right)\frac{\mu_\beta^2}{\rho_\beta \ell^3} = C \quad \text{for all } Y \tag{11g}$$

where the dimensionless constant $C$, is used to define the magnitude of the pressure drop, which must be small enough to satisfy the Stokes flow assumption. In Eqs. (11), $\nabla$ indicates the dimensionless differential operator.

Following Eidsath et al. (1983), to generate the flow field, the dimensionless local pressure is decomposed according to

$$p = \langle p \rangle_{ds}^\beta + \tilde{p} \tag{12}$$

Here $\langle p \rangle_{ds}^\beta$, is the intrinsic average of $p$, that must be evaluated according to

$$\langle p \rangle_{ds}^\beta = \frac{1}{V_{\beta,ds}} \int_{\mathscr{V}_{\beta,ds}} p dV \tag{13}$$

where $\mathscr{V}_{\beta,ds}$ is the fluid locus in the periodic solution domain shown in Fig. 4. Furthermore, the pressure deviation $\tilde{p}$, that was introduced in Eq. (12), must satisfy the restriction

$$\langle \tilde{p} \rangle_{ds}^\beta = 0 \tag{14}$$

Since the pressure drop, given by Eq. (7d), is constant in the bulk of both homogeneous regions, the dimensionless pressure drop may be written as

$$\nabla \langle p \rangle^\beta = -C\mathbf{i} \tag{15}$$

At this point, the local problem that must be solved in the free fluid/porous medium system is totally defined, and it is the following

$$\nabla \cdot \mathbf{u} = 0 \quad \beta - \text{phase} \tag{16a}$$

$$\mathbf{0} = -\nabla \tilde{p} + C\mathbf{i} + \nabla^2 \mathbf{u} \quad \beta - \text{phase} \tag{16b}$$

B. C. 1 $$\mathbf{u} = \mathbf{0} \quad \text{at} \quad \mathscr{A}_{\beta\sigma} \tag{16c}$$

B. C. 2 $$\mathbf{u} = \mathbf{0} \quad \text{at} \quad Y = L_\eta/\ell \tag{16d}$$

B. C. 3 $$\mathbf{n}_\beta \cdot (\nabla \mathbf{u}) = \mathbf{0} \quad \text{at} \quad Y = -L_\omega/\ell \tag{16e}$$

$$\mathbf{u}(\mathbf{r}/\ell) = \mathbf{u}(\mathbf{r}/\ell + \mathbf{i}) \tag{16f}$$

$$\tilde{p}(\mathbf{r}/\ell) = \tilde{p}(\mathbf{r}/\ell + \mathbf{i}) \tag{16g}$$

The solution of this problem is carried out using the finite element solver COMSOL Multiphysics 5.2. The porosity of the bulk of the porous medium, $\varepsilon_{\beta\omega}$, depends on the configuration in each of the unit cells shown in Fig. 3, and its value is obtained once the ratio $\ell_\sigma/\ell$ is fixed. It should be noted that if $C = 0$ the problem becomes homogeneous. In this way, due to the linearity of the boundary value problem, it is only necessary to solve for one value of $C$, the solutions for other values can be obtained by the appropriate up-scaling.

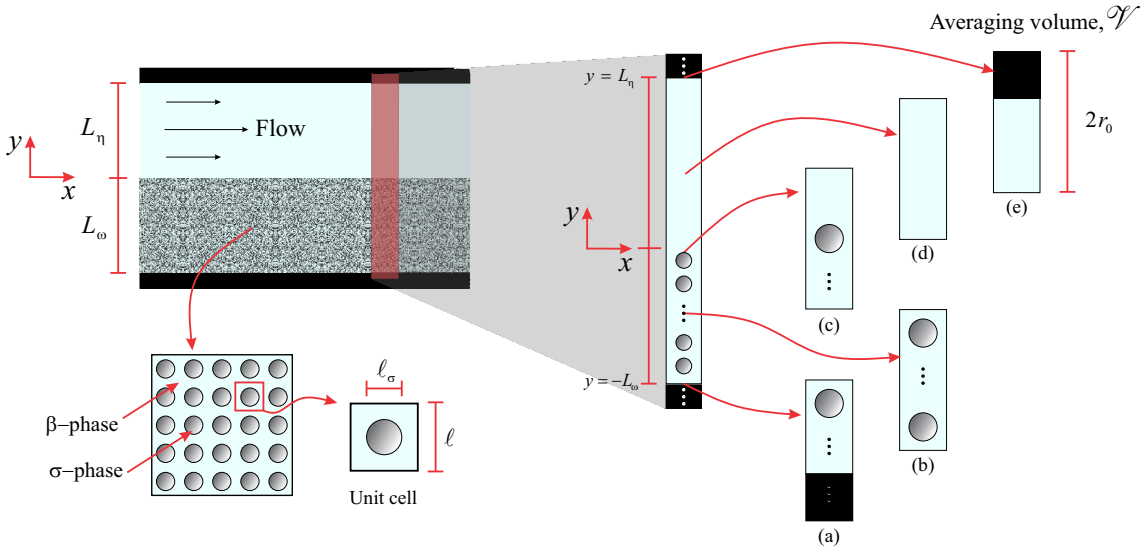


Fig. 4. Periodic domain for the solution of the pore-scale problem. The samples in different regions of the periodic domain are shown in the: (a) wall/porous medium inter-region, (b) homogeneous porous medium, (c) fluid/porous medium inter-region, (d) homogeneous fluid region, and (e) fluid/wall inter-region.

For the calculations, we considered a channel with $L_\eta = 10^3\ell$ and $L_\omega = 10^2\ell$. Thus, the complete height of the channel is $L_\eta + L_\omega = 1.1 \text{ x } 10^3\ell$. In general, this leads to a disparity of characteristic length-scales of at least two orders of magnitude between the pore-scale and the macroscopic system, which satisfies that $\ell \ll L_\eta, L_\omega$.

The statement of the flow problem, given by eqs. (16), shows that the intention of this paper is to restrict the analysis to non-inertial flow cases. However, it is worth to analyze that, if there are some cases in which, even when in the bulks of the homogeneous regions the flow is non-inertial, the flow is inertial in the inter-region. This analysis is carried out in the following subsection.

## 2.3 *Limit of application of Stokes flow model in the channel system*

In the following paragraphs, the maximum value of $C$ for which Eq. (16b) can be used is determined. To this end, the DNS results obtained with the eqs. (16) are compared with the ones obtained when Eq. (16b) is replaced by the dimensionless Navier-Stokes (N-S) equation, given by

$$\mathbf{u}\cdot\nabla\mathbf{u} = -\nabla\tilde{p} + C\mathbf{i} + \nabla^2\mathbf{u}, \qquad \text{in the } \beta-\text{phase} \quad (17)$$

In Table 1, the maximum difference percentages between the velocity magnitudes obtained with Navier Stokes and Stokes models are reported for different values of the dimensionless pressure drop and two values of $\varepsilon_{\beta\omega}$. As it should be, the difference percentage between the results obtained with the two models increases as $C$ is augmented. In the row for $C = 10^{-5}$, it can be observed that, the difference percentage between the results obtained with the two models is no larger than $1.2\text{x}10^{-3}$. This suggests that, the inertial contributions can be neglected for $C \leq 10^{-5}$. It is worth mentioning, that the largest differences between the two model predictions are found in the free fluid/porous medium inter-region.

In addition, some of the results obtained for the flow in the free fluid/porous medium inter-region with the N-S equation, for different values of $C$, are shown in figs. 5 and 6. In the first of them, Fig. 5, it is apparent that the shape of the contour plots for the velocity magnitude obtained with $C = 10^{-5}$ and $C = 10^{-4}$ are the same; it could be said that, the field corresponding to $C = 10^{-4}$ is almost the same that the one for $C = 10^{-5}$ multiplied by 10. Then, if one is willing to accept the error indicated in Table 1, the inertial contributions could be neglected even for $C \leq 10^{-4}$. In figs. 5c and d the distortion of the flow fields, for $C = 0.1$ and $C = 1$ with respect to $C = 10^{-5}$ are much more evident. The previous comments are confirmed by the comparison of the streamlines shown in Fig. 6. There is not a noticeable difference between the figs. 6a and

Table 1. Maximum difference percentage between the local velocities predicted by Navier-Stokes and Stokes models for different values of the dimensionless pressure drop, $C$. The results are for cylindrical particles, $L_\eta = 10^3\ell$ and $L_\omega = 10^2\ell$.

| $C$ | $\varepsilon_{\beta\omega} = 0.4$ | $\varepsilon_{\beta\omega} = 0.8$ |
|---|---|---|
| $10^{-5}$ | 0.00120 | $1.61x10^{-4}$ |
| $10^{-4}$ | 0.01204 | $1.61x10^{-3}$ |
| $10^{-3}$ | 0.12090 | $1.63x10^{-2}$ |
| $10^{-2}$ | 1.22278 | $1.67x10^{-1}$ |
| 0.1 | 8.25514 | 4.91 |
| 1 | 18.6852 | 19.29 |

b. However, the stream lines behavior for $C = 0.1$ and $C = 1$ around the two solid particles in contact with the free fluid are clearly different. Navier-Stokes model must be used for these values of $C$. It should be emphasized that, the results are for the particular configuration shown in Fig. 4 and may depend on $L_\eta/\ell$.

In the following paragraphs, using the information from the DNS for the channel system, we evaluate the Reynolds numbers in the bulk of the homogeneous regions which are given by

$$\mathrm{Re}_\eta = \frac{\rho_\beta v_{\beta,max} L_\eta}{\mu_\beta}, \qquad \mathrm{Re}_{p\omega} = \frac{\rho_\beta \langle v_\beta \rangle_\omega d}{\mu_\beta} \tag{18}$$

where $v_{\beta,max}$ and $\langle v_\beta \rangle_\omega$ are the maximum velocity in the free flow region and the superficial average velocity in the bulk of the porous medium, respectively. These results will help in further studies to determine when can the flow be treated as non-inertial in the whole channel domain. In this way, by using Eq.(10), the Reynolds numbers can also be written as follows

$$\mathrm{Re}_\eta = \frac{L_\eta u_{max}}{\ell} \tag{19}$$

$$\mathrm{Re}_{p\omega} = \frac{\ell_\sigma}{\ell}\frac{K_{\beta\omega}}{\ell^2} C \tag{20}$$

In this last equation, Darcy's law has been used to replace $\langle v_\beta \rangle_\omega$. In order to evaluate $\mathrm{Re}_{p\omega}$, for a given $C$, it is necessary to know $K_{\beta\omega}$, which can be obtained, as explained latter in Sec. *3.3*, for a given porous medium microstructure and $\varepsilon_{\beta\omega}$. However, the evaluation of $Re_\eta$ requieres the solution of the Stokes problem to obtain $u_{max}$ once $L_\eta/\ell$ is fixed.

In Table 2 the values of both Reynolds numbers for the bulks of the homogeneous regions are reported. The values indicate the conservative upper limit for the use of Stokes model in the bulk of the free fluid and in the bulk of the porous medium. In addition, in Table 3 the Reynolds number for different positions inside the inter-region are shown. These values indicate that the flow around the first and second solid particle may not correspond to Stokes regime.

Table 2. Reynolds numbers of both homogeneous regions of the channel partially filled with a porous medium for several values of $\varepsilon_{\beta\omega}$. The results are for cylindrical particles, $C = 10^{-5}$, $L_\eta = 10^3\ell$, and $L_\omega = 10^2\ell$.

| $\varepsilon_{\beta\omega}$ | $\mathrm{Re}_{p\omega}$ | $\mathrm{Re}_\eta$ |
|---|---|---|
| 0.3 | $6.98\text{x}10^{-10}$ | 1250 |
| 0.4 | $4.96\text{x}10^{-9}$ | 1250 |
| 0.5 | $1.50\text{x}10^{-8}$ | 1251 |
| 0.6 | $3.28\text{x}10^{-8}$ | 1251 |
| 0.7 | $6.00\text{x}10^{-8}$ | 1251 |
| 0.8 | $9.79\text{x}10^{-8}$ | 1251 |
| 0.9 | $1.44\text{x}10^{-7}$ | 1251 |

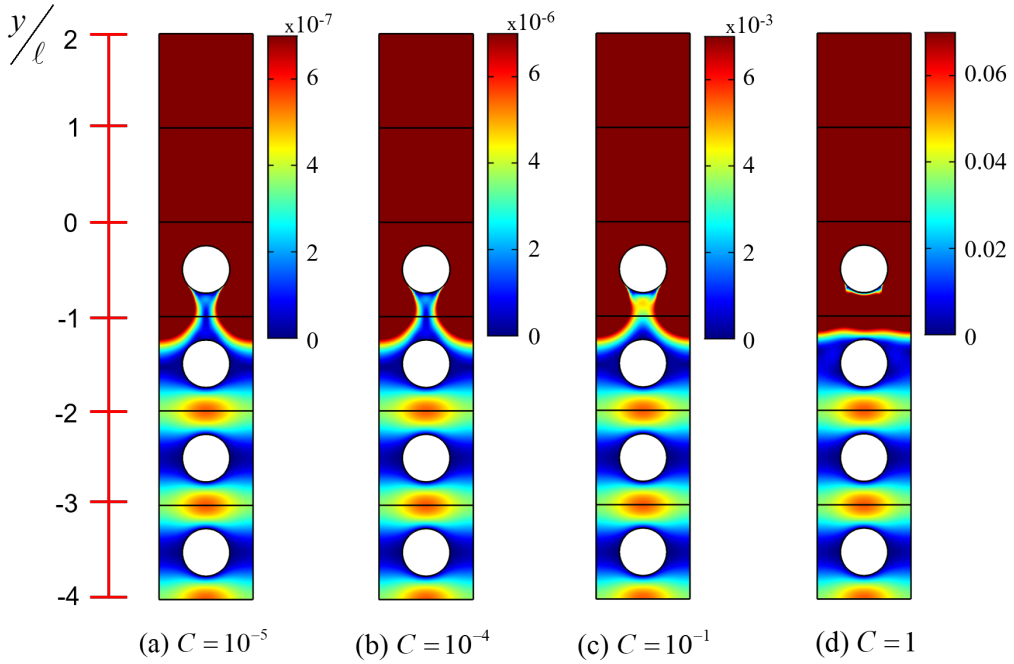


Fig. 5. Effect of the dimensionless pressure drop, $C$, on the local velocity magnitude in a neighborhood of the free fluid/porous medium inter-region predicted by the Navier-Stokes equation model. The DNS is for cylindrical particles, $L_\eta = 10^3\ell$, $L_\omega = 10^2\ell$, and $\varepsilon_{\beta\omega} = 0.8$.

Table 3. Particle Reynolds numbers in the free fluid/porous medium inter-region using a porous medium made of cylinders in line for different values of the dimensionless pressure drop, $C$. In all the calculations we used $L_\eta = 10^3\ell$, $L_\omega = 10^2\ell$, and two values of $\varepsilon_{\beta\omega}$.

| | | $Re_p(y/\ell)$ | | | |
|---|---|---|---|---|---|
| $\varepsilon_{\beta\omega}$ | $y/\ell$ | $C = 10^{-5}$ | $C = 10^{-4}$ | $C = 0.1$ | $C = 1$ |
| 0.4 | 1.5 | 7.01 x$10^{-3}$ | 7.01 x$10^{-2}$ | 70.0 | 697 |
| | 0.5 | 2.65 x$10^{-3}$ | 2.65 x$10^{-2}$ | 26.4 | 261 |
| | -0.5 | 7.41 x$10^{-5}$ | 7.41 x$10^{-4}$ | 0.70 | 5.51 |
| | -1.5 | 1.24 x$10^{-8}$ | 1.24 x$10^{-7}$ | 1.24 x$10^{-4}$ | 1.24x$10^{-3}$ |
| | -2.5 | 1.24 x$10^{-8}$ | 1.24 x$10^{-7}$ | 1.24 x$10^{-4}$ | 1.24x$10^{-3}$ |
| 0.8 | 1.5 | 4.54x$10^{-3}$ | 4.54x$10^{-2}$ | 45.3 | 451 |
| | 0.5 | 2.02x$10^{-3}$ | 2.02x$10^{-2}$ | 20.1 | 200 |
| | -0.5 | 1.48x$10^{-4}$ | 1.48x$10^{-3}$ | 1.44 | 13.1 |
| | -1.5 | 5.31x$10^{-8}$ | 5.31x$10^{-7}$ | 5.58x$10^{-4}$ | 6.31x$10^{-3}$ |
| | -2.5 | 1.23x$10^{-7}$ | 1.23x$10^{-6}$ | 1.23x$10^{-3}$ | 1.23x$10^{-2}$ |

## 2.4 *Average velocity profile from direct numerical simulations*

In order to analyze the flow in the free fluid/porous medium system at the macroscale (*i.e.*, at Darcy's scale), in the following lines we obtain the average velocity profiles by averaging the local velocity profiles. The averaging volume that could be used for this purpose is shown in the Fig. 2. Nevertheless, due to the periodic geometry of the subdomain used for the DNS, it is convenient to choose as the averaging volume a parallelepiped with a rectangular cross-sectional area tangent to the main flow direction, such as the one shown in Fig. 4. The cross-sectional area

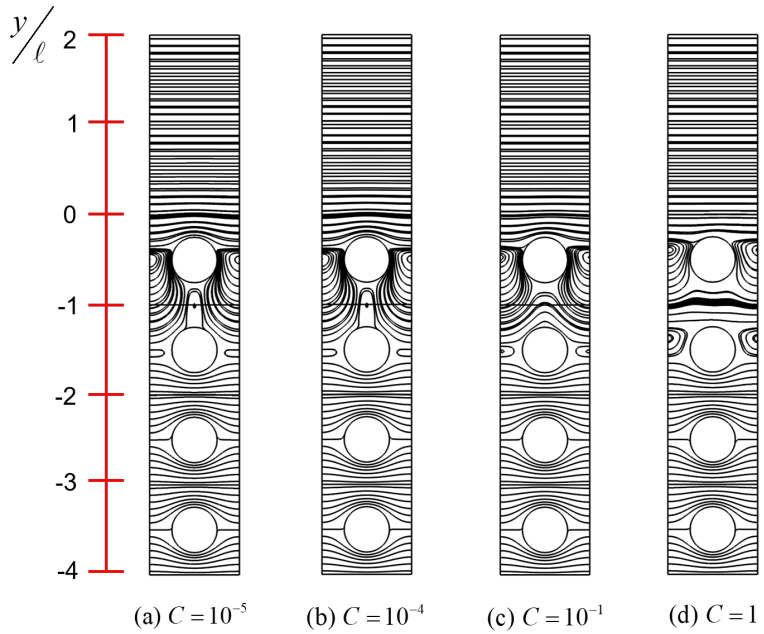


Fig. 6. Effect of the dimensionless pressure drop, $C$, on the stream lines in the neighborhood of the free fluid/porous medium inter-region predicted by the Navier-Stokes equation model. The DNS is for cylindrical particles, $L_\eta = 10^3\ell$, $L_\omega = 10^2\ell$, and $\varepsilon_{\beta\omega} = 0.8$.

of the averaging domain is $2r_0\ell$, where $r_0$ is one half of the height of the samples and $\ell$ is the width of the samples. In this way, the intrinsic average operator, given by (2b), may be written as

$$\langle u_x\rangle^\beta|_{y_0} = \frac{1}{\varepsilon_\beta(y_0)2r_0\ell}\int_{y=y_0-r_0}^{y=y_0+r_0}\int_{x=x_0-\frac{1}{2}\ell}^{x=x_0+\frac{1}{2}\ell} m_\beta(\mathbf{r})u_x(x,y)\,dxdy \tag{21}$$

where $m_\beta(\mathbf{r})$ is a phase indicator function defined as

$$m_\beta(\mathbf{r}) = \begin{cases} 1 & \text{if } \mathbf{r} \in \mathscr{V}_\beta(\mathbf{x}) \\ 0 & \text{if } \mathbf{r} \notin \mathscr{V}_\beta(\mathbf{x}) \end{cases} \tag{22}$$

Notice that, we are only interested in obtaining the component of the dimensionless velocity in the direction of the pressure drop, namely $u_x = \mathbf{u}\cdot\mathbf{i}$. This is because the main changes of the velocity profile at the macroscale are along this direction. In this way, we obtained the average velocity profile along the vertical direction using the Eq. (21). In the following paragraphs, the average velocity results will be presented as follows

$$u^* = \frac{\langle u_x\rangle^\beta}{u_{max}} \tag{23}$$

where $u_{max} = \max\left(\langle u_x\rangle^\beta\right)$. In Fig. 7, the average velocity profiles resulting from DNS, for $\varepsilon_{\beta\omega} = 0.4$ and five sample sizes $r_0/\ell$ (1, 2, 5, 10 and 15) are reported. In Fig. 7a, we show the superimposed average velocity profiles in the whole domain of the channel for three microstructures of the porous medium. However, at this level of amplification, it is not possible to categorically conclude if the size of the averaging volume or the microstructure of the porous medium have some significant effect on the average velocity profiles. For that reason, in Fig. 7b , the close up of the profiles in the neighborhood of the maximum velocity is shown.

Then, it is clear that, for the same fluid volume fraction, there is not a significant effect of the porous medium configuration or the sample size on any of the velocity profiles in the free flow part of the system. Finally, in Fig. 7c, the close up of the average velocity profiles in the free fluid/porous medium inter-region $-r_0 \leq y \leq r_0$ is shown. Note that, at $y = 0$ the clear fluid ends, therefore, the samples corresponding to $y \geq +r_0$ are fully located in the fluid and the ones for $y \leq -r_0$ are fully located in the porous medium. These results show that the velocity profiles take Darcy's velocity value for $y \lesssim -r_0$. Therefore, the thickness of Brinkman's layer is approximately $r_0$.

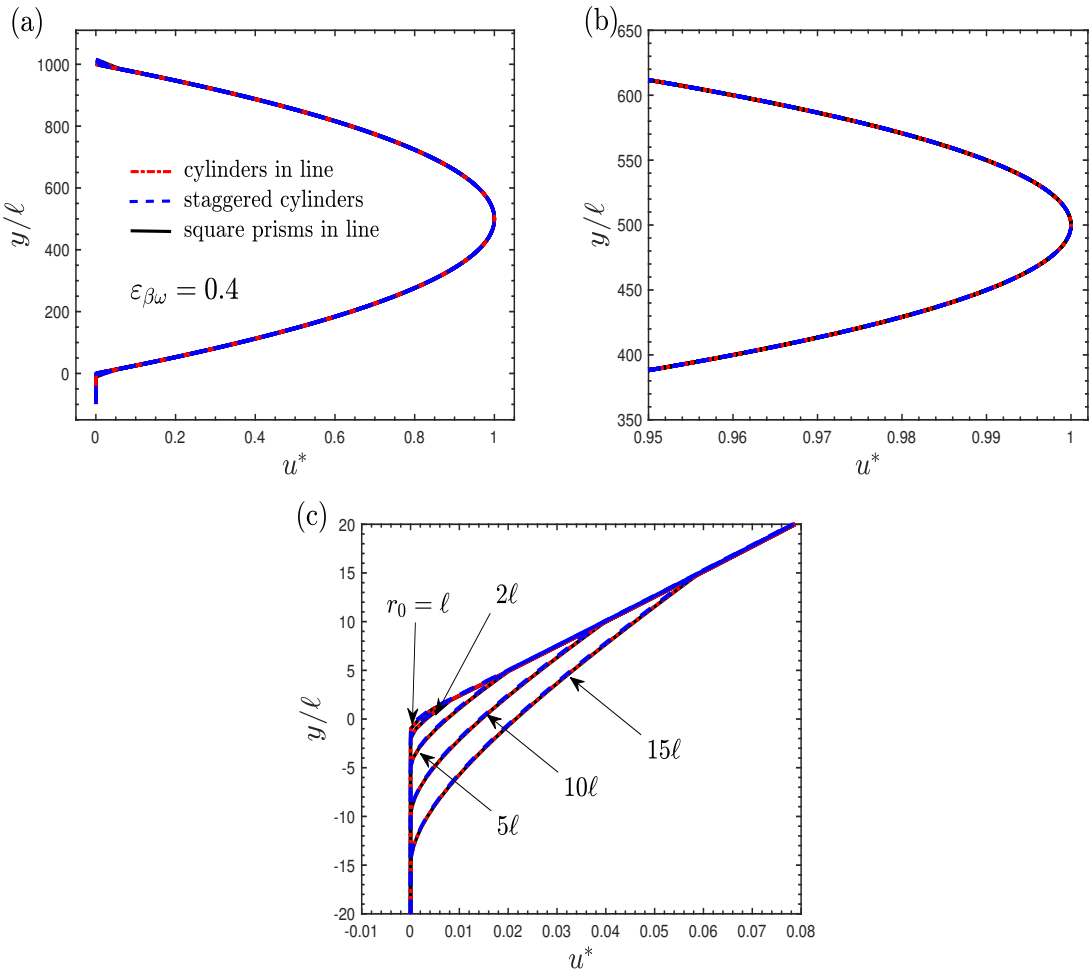


Fig. 7. Intrinsic average velocity profiles obtained from DNS for a channel partially filled with a particulate porous medium. For (a) the open gap of the channel and part of the porous medium, (b) the maximum velocity region, and (c) the free fluid/porous medium inter-region. In all simulations we fixed $C = 10^{-5}$, $L_\eta = 10^3\ell$, $L_\omega = 10^2\ell$, and $\varepsilon_{\beta\omega} = 0.4$. The sample sizes $r_0$ are the reported in Part (c) of this figure.

In the same way, for most of the channel system, there is not a noticeable difference when comparing the DNS average velocity profiles shown in Fig. 7, with ones obtained from the analytic expressions for stratified porous medium formed by parallel cylindrical capillary pores (Ochoa-Tapia et al., 2017) and the corresponding to stratified porous medium formed by parallel plates reported in Appendix A of this paper. Even more, as it is shown in Fig. 8, the DNS and analytic results also coincide in the inter-region.

In addition, the comparison of the velocity profiles obtained for different $\varepsilon_{\beta\omega}$ values shows negligible differences almost for the whole channel system. For such reason, we limit the comparison of the predictions to the inter-region neighborhood where, at this level of amplification, appreciable differences are located. This can be observed in Fig. 9, where the results already shown above for $\varepsilon_{\beta\omega} = 0.4$ are compared with the values corresponding to $\varepsilon_{\beta\omega} = 0.8$. It should be noted that, in the arithmetic scale that is used in figs. 7 to 9, the values for the average velocity corresponding to the bulk of the porous media $\langle u_x \rangle_\omega^\beta$, although, they are about $10^{-7}$, seem like zero. This is shown in detail in Table 4, where $\langle u_x \rangle_\omega^\beta$ is compared with the intrinsic average velocities at $y = 0$ for the different porous media microestructures and sample

sizes. Note that each one of the $\langle u_x \rangle_\omega^\beta$ is negligible with respect to all values $\langle u_x \rangle^\beta|_{y=0}$. The same type of results are obtained for other bulk fluid volume fractions, $0.1 \leq \varepsilon_{\beta\omega} \leq 0.9$. It is precisely, the difference between the $\langle u_x \rangle_\omega^\beta$ for a given $\varepsilon_{\beta\omega}$ which leads to the differences between the average velocity profiles for $\varepsilon_{\beta\omega} = 0.4$ and $\varepsilon_{\beta\omega} = 0.8$ shown in Fig. 9. This is because the average velocity at $y = 0$ is directly related to the arithmetic average of the flow rates for the free fluid and porous medium contained by the corresponding sample. However, given that $L_\eta = 10^3\ell$, the inter-region effect is not enough to yield different values for the maximum velocity and its location in the free flow region. Then, for the dimensionless pressure drop $C = 10^{-5}$ and each one of the bulk porosity values, it was found that $u_{max} \approx 1.25$ at $Y \approx 0.5L_\eta/\ell$. Later, in the Discussion Section, this situation will be further elaborated in terms of the analytic expressions presented for the stratified parallel plates porous media model and other findings of the following sections. Finally, in Fig. 10 part of the DNS volume average results shown in Fig. 9 ($r_0 = \ell, 15\ell$) are compared with the $x$-average velocity profiles for two values of $\varepsilon_{\beta\omega}$. The $x$-average, for a given value of $y_0$, was evaluated following the definition

$$\hat{u}_x^\beta|_{y_0} = \frac{1}{\hat{\varepsilon}_\beta|_{y_0}\ell} \int_{x=x_0-\frac{1}{2}\ell}^{x=x_0+\frac{1}{2}\ell} m_\beta(\mathbf{r}) u_x(x, y_0)\, dx \tag{24}$$

where $\hat{\varepsilon}_\beta$, the fraction of $\ell$ that is occupied by the fluid, is given by

$$\hat{\varepsilon}_\beta|_{y_0} = \frac{1}{\ell} \int_{x=x_0-\frac{1}{2}\ell}^{x=x_0+\frac{1}{2}\ell} m_\beta(\mathbf{r}) dx \tag{25}$$

At the level of amplification used in these figures there is not noticeable difference between the $x$-average and the volume average profile corresponding to $r_0 = \ell$. However, the difference becomes evident as $r_0$ increases.

All the observations in this section, on the effect of the free fluid flow on the porous media velocity profile, are in terms of average velocity. This raises some questions on the analogous effect in terms of the local velocity distribution. In the following sections, using the local velocity results from the DNS, we determine the extension of the influence of the free fluid motion on the flow inside of the porous medium and of the disturbance zone in the free fluid due to the flow in the porous medium.

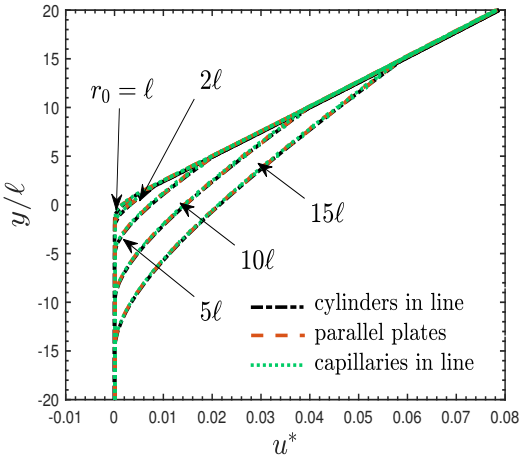


Fig. 8. Average velocity profiles in the free fluid/porous medium inter-region as function of the sample size, $r_0$. The calculations are for the porous media formed by cylinders in line, parallel plates, and capillaries in line. In all the simulations $C = 10^{-5}$, $L_\eta = 10^3\ell$, $L_\omega = 10^2\ell$, and $\varepsilon_{\beta\omega} = 0.4$.

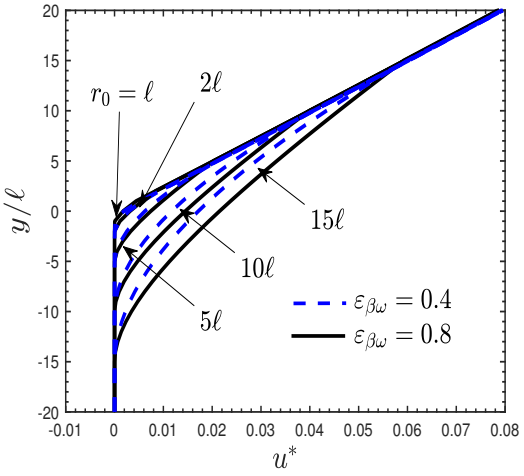


Fig. 9. Intrinsic average velocity profiles in the free fluid/porous medium inter-region as function of $\varepsilon_{\beta\omega}$ and the sample size, $r_0$. All DNS results are for porous media made of cylinders in line with $C = 10^{-5}$, $L_\eta = 10^3\ell$, and $L_\omega = 10^2\ell$.

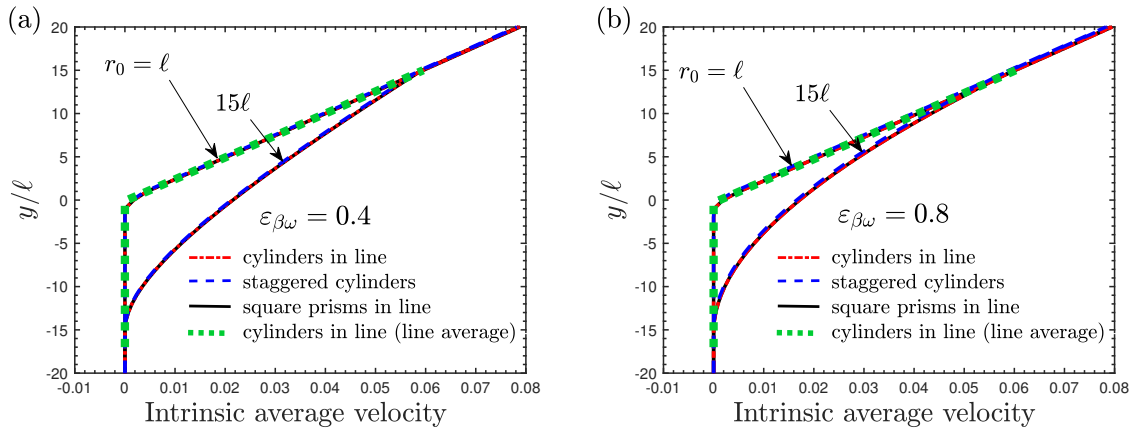


Fig. 10. Comparison of the intrinsic volume average and intrinsic line average velocities in the free fluid-porous medium inter/region for two values of $\varepsilon_{\beta\omega}$. All DNS results are $C = 10^{-5}$, $L_\eta = 10^3\ell$, and $L_\omega = 10^2\ell$.

## 3 Effect of the flow in one homogeneous region on the local velocity profile of the adjacent region

As shown above, a smooth transition zone in the average velocity profiles exists at the free fluid/porous medium inter-region. The size of the part located inside the porous medium is approximately $r_0$. This transition zone is found even for consolidated porous media models like the capillary and parallel plates cases. It is clear that the average velocity profiles previously presented depend on the DNS results. However, the solution of the local model is independent of the shape and size of the sample, therefore the following analysis is not related to the averaging process. Then, it is worth to note, as it is shown in Fig. 6, that inside the free fluid, the stream lines are horizontal far enough from the solid particles. In addition, as it is also shown in Fig. 6, one should realize that the shape of the stream lines around each solid particle look alike as one moves inside the porous

medium. Thus, in terms of the local velocity, the effect of the solid particles in the porous medium on the free fluid flow is lost at certain distance ($d_\eta$) inside the homogeneous free fluid. Analogously, the effect of the free fluid motion must vanish at certain distance ($d_\omega$) inside the porous medium bed. In the following lines we describe the procedures that were followed to determine the values for both $d_\omega$ and $d_\eta$, which are shown in Fig. 11.

### *3.1 Determination of $d_\eta$ and $d_\omega$*

In one hand, to determine $d_\eta$, it is crucial to recognize that far enough from the solid particles of the porous medium, the motion of the fluid is essentially parallel to the upper wall: $\mathbf{u}\cdot\mathbf{i} = u_x(y) \neq 0$ and $\mathbf{u}\cdot\mathbf{j} = u_y = 0$. For such reason, for $y \geq d_\eta$, $u_x$ only depends on the vertical coordinate, $y$. Therefore, $d_\eta$ is the value of the vertical coordinate where all the local horizontal velocity profiles begin to superimpose one over the

Table 4. Dimensionless intrinsic average velocity at $y = 0$ for different porous medium models and two values of $\varepsilon_{\beta\omega}$. The dimensionless pressure drop $C$, $L_\eta$ and $L_\omega$ are $10^{-5}$, $10^3\ell$, and $10^2\ell$, respectively.

| $r_0/\ell$ | cylinders in line | staggered cylinders | square prisms in line | parallel plates | capillaries in line |
|---|---|---|---|---|---|
| $\varepsilon_{\beta\omega} = 0.4$ | | | | | |
| 1 | $2.19\text{x}10^{-3}$ | $1.82\text{x}10^{-3}$ | $2.22\text{x}10^{-3}$ | $1.78\text{x}10^{-3}$ | $1.78\text{x}10^{-3}$ |
| 2 | $3.96\text{x}10^{-3}$ | $3.60\text{x}10^{-3}$ | $3.99\text{x}10^{-3}$ | $3.57\text{x}10^{-3}$ | $3.57\text{x}10^{-3}$ |
| 5 | $9.28\text{x}10^{-3}$ | $8.93\text{x}10^{-3}$ | $9.32\text{x}10^{-3}$ | $8.90\text{x}10^{-3}$ | $8.90\text{x}10^{-3}$ |
| 10 | $1.81\text{x}10^{-2}$ | $1.78\text{x}10^{-2}$ | $1.82\text{x}10^{-2}$ | $1.77\text{x}10^{-2}$ | $1.77\text{x}10^{-3}$ |
| 15 | $2.69\text{x}10^{-2}$ | $2.66\text{x}10^{-2}$ | $2.69\text{x}10^{-2}$ | $2.65\text{x}10^{-2}$ | $2.65\text{x}10^{-2}$ |
| $\langle u_x\rangle^\beta_\omega$ | $1.42\text{x}10^{-8}$ | $7.09\text{x}10^{-9}$ | $2.62\text{x}10^{-8}$ | $1.07\text{x}10^{-7}$ | $1.59\text{x}10^{-7}$ |
| $\varepsilon_{\beta\omega} = 0.8$ | | | | | |
| 1 | $2.36\text{x}10^{-3}$ | $1.49\text{x}10^{-3}$ | $2.34\text{x}10^{-3}$ | $1.39\text{x}10^{-3}$ | $1.39\ \text{x}10^{-3}$ |
| 2 | $3.68\text{x}10^{-3}$ | $2.87\text{x}10^{-3}$ | $3.66\ \text{x}10^{-3}$ | $2.77\text{x}10^{-3}$ | $2.77\ \text{x}10^{-3}$ |
| 5 | $7.78\text{x}10^{-3}$ | $7.02\text{x}10^{-3}$ | $7.77\text{x}10^{-3}$ | $6.92\text{x}10^{-3}$ | $6.92\ \text{x}10^{-3}$ |
| 10 | $1.46\text{x}10^{-2}$ | $1.39\text{x}10^{-2}$ | $1.46\text{x}10^{-2}$ | $1.38\text{x}10^{-2}$ | $1.38\ \text{x}10^{-2}$ |
| 15 | $2.15\text{x}10^{-2}$ | $2.07\text{x}10^{-2}$ | $2.15\text{x}10^{-2}$ | $2.06\text{x}10^{-2}$ | $2.06\ \text{x}10^{-2}$ |
| $\langle u_x\rangle^\beta_\omega$ | $2.43\text{x}10^{-7}$ | $1.21\text{x}10^{-8}$ | $2.26\text{x}10^{-7}$ | $4.27\text{x}10^{-7}$ | $3.18\text{x}10^{-7}$ |

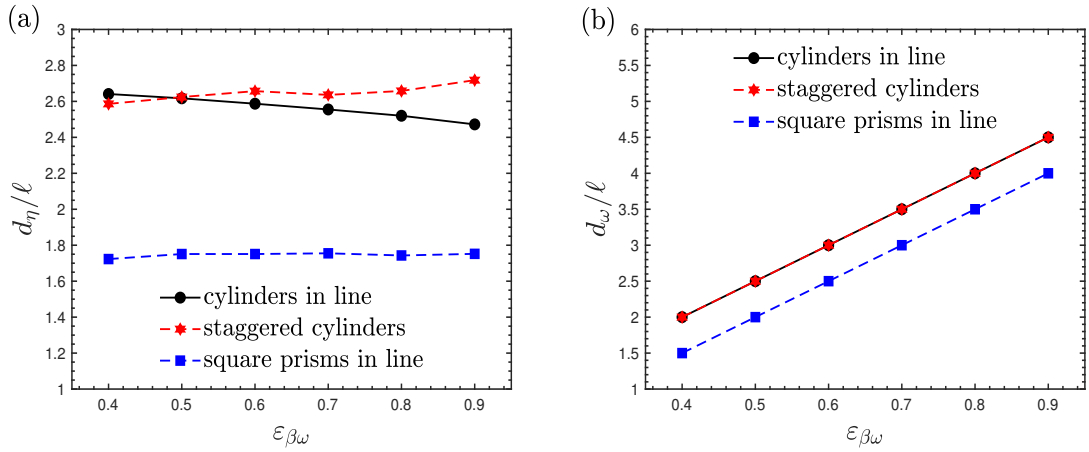


Fig. 11. Effect of $\varepsilon_{\beta\omega}$ on: (a) the distance where the flow in the free fluid region becomes one-dimensional (*i.e.*, $d_\eta$), and (b) distance inside of the porous medium in which the free fluid flow effect is lost (*i.e.*, $d_\omega$). Both distances are measured from the end of the unit cell in contact with the free fluid. All the DNS results are for $C = 10^{-5}$, $L_\eta = 10^3\ell$, and $L_\omega = 10^2\ell$.

other. From that position, until reaching the upper wall, only one curve is needed to represent $u_x$. The outlined procedure was used to compare the DNS local velocity profiles for $X = 0, 0.25$ and $0.5$. Then, $d_\eta$ is the smallest value of $Y$ for which the percentage difference between the three values of the local velocity component, $u_x$ is less than $10^{-3}$.

On the other hand, to estimate $d_\omega$, one must accept that, at certain distance inside the porous medium, the presence of the free flow is lost. As a consequence, the local velocity distribution far enough from the free fluid is obtained by solving the flow problem given by eqs. (7) in one unit cell where periodic boundary conditions are enforced. In this way, $d_\omega$ can be determined by comparing the local velocity profiles obtained from the DNS for each unit cell of the whole system with the corresponding to a unit cell of the bulk. Therefore, $d_\omega$ was determined by the smallest value of $-y$ for which the difference percentage between the two mentioned velocity profiles is less than $10^{-3}$. The comparison was carried out only for $Y =$ multiples of $-\frac{1}{2}$. The results for $d_\eta$ and $d_\omega$, as a function of the bulk fluid volume fraction $\varepsilon_{\beta\omega}$ are shown in Fig. 11. It can be said that, for the channel system and the three porous medium configurations here considered, the effect of the porous media on the free flow is lost for $y \geq 3\ell$ and the effect of the free flow on the porous media is lost for $y \leq -5\ell$.

## 3.2 *The local velocity profile in the undisturbed free fluid region*

In the previous section, we determined the extension of the effect that one region may have on the other in the free fluid/porous medium system shown in Fig. 2. There we have found that the distance of the disturbance of the flow in the free fluid region due to the presence of the porous medium is about three times the size of a unit cell over the surface of the porous medium.

As a consequence, since the flow is totally developed, for $Y \in \left[d_\eta/\ell, L_\eta/\ell\right]$, the problem given by eqs. (11) may be reduced to

$$0 = C + \frac{d^2\langle u_x\rangle^\beta}{dY^2} \tag{26}$$

which is subject to the boundary conditions given by

$$\langle u_x\rangle^\beta = 0 \quad \text{at} \quad Y = L_\eta/\ell \tag{27}$$

$$\langle u_x\rangle^\beta = u_\eta \quad \text{at} \quad Y = d_\eta/\ell \tag{28}$$

where $u_\eta$ is the velocity at the position $Y = d_\eta/\ell$ that may be determined following the procedure described above for the DNS. Furthermore, in Eq. (26), we have replaced the dimensionless pressure drop by $C$ according to Eq. (15). In this way, the velocity profile in the unperturbed free flow region is given by

$$\langle u_x\rangle^\beta = -\frac{1}{2}C\left(Y - \frac{L_\eta}{\ell}\right)\left(Y - \frac{d_\eta}{\ell}\right) + u_\eta\left(\frac{Y - L_\eta/\ell}{d_\eta/\ell - L_\eta/\ell}\right) \tag{29}$$

where, it is possible to identify the Poiseuille and Couette flow type contributions. In Fig. 12a, we show the comparison of the local velocity profiles obtained in a cut line at $X = 0$ (position located at half of the distance between adjacent particles in the unit cell centers) from the DNS with those predicted using Eq. (29). The results were obtained for $\varepsilon_{\beta\omega} = 0.8$ and porous medium made of cylindrical particles (see Fig. 3a). The observation of figs. 12a and b shows that no visual differences can be appreciated at the level of the whole channel or in the close up of the maximum velocity neighborhood. Moreover, the comparison is also very good in a vicinity of $y = d_\eta$ (Fig. 12c) where the domain for which $u_y = 0$ starts . This is confirmed by the evaluation of the relative error percentage defined by

$$\text{Error } \% = \frac{\left|\langle u_x\rangle^\beta\big|_{DNS} - \langle u_x\rangle^\beta\big|_{\text{Eq.(29)}}\right|}{\langle u_x\rangle^\beta\big|_{\text{Eq.(29)}}}\text{x}100\% \tag{30}$$

that was found to be of the order of $10^{-8}$. The same kind of results were obtained using the other porous media geometries shown in Fig. 3. Therefore, the use of Eq. (29) could help in a more DNS efficient numerical scheme to avoid the numerical solution in large part of the channel system. Finally, it should be mentioned that, since $r_0/L_\eta \leq 0.015$ in all calculations, Eq. (29) can be used to represent also the horizontal component of the average velocity, $\langle u_x\rangle^\beta$ (see Eq. (5)).

## 3.3 *The Brinkman boundary layer and its relationship to the permeability of the bulk of the porous medium*

As mentioned above, the Brinkman boundary layer is defined as the zone in the average velocity profile where velocity decreases drastically from the velocity at the surface of the porous medium ($y = 0$) until reaching the value of Darcy's velocity (Neale and Nader, 1974). The determination of the extension of this transition zone ($\delta_B$) has received large attention in literature (Goharzadeh et al., 2005; Goyeau et al.,

2003; Morad and Khalili, 2009; Ochoa-Tapia and Whitaker, 1995a,b; Sahraoui and Kaviany, 1992). In several works, it has been mentioned that if Brinkman's transition zone exist, it is of the order of the square root of the permeability of the porous medium bulk ($\sqrt{K_{\beta\omega}}$). Lines above, we found that the Brinkman boundary layer exists, and its size is of the order of one half of the characteristic length of the sample (*i.e.*, $\delta_B = r_0$). In this section, we use our findings to evaluate $\delta_B/\sqrt{K_{\beta\omega}} = r_0/\sqrt{K_{\beta\omega}}$ as a function of the porosity, $\varepsilon_{\beta\omega}$.

Then, it is first necessary to determine the permeability of the bulk of the porous medium. In this work, it is obtained using the one-dimensional version of Eq. (1), with $\langle v_{\beta x}\rangle_\omega$ from the DNS in a unit cell for a given pressure drop. Thus, the flow boundary value problem that must be solved is analogous to that given by eqs. (16) where eqs. (16d) and (16e) are replaced by periodic boundary conditions. Some examples of the local velocity profiles are shown in Fig. 13 for different values of $\varepsilon_{\beta\omega}$.

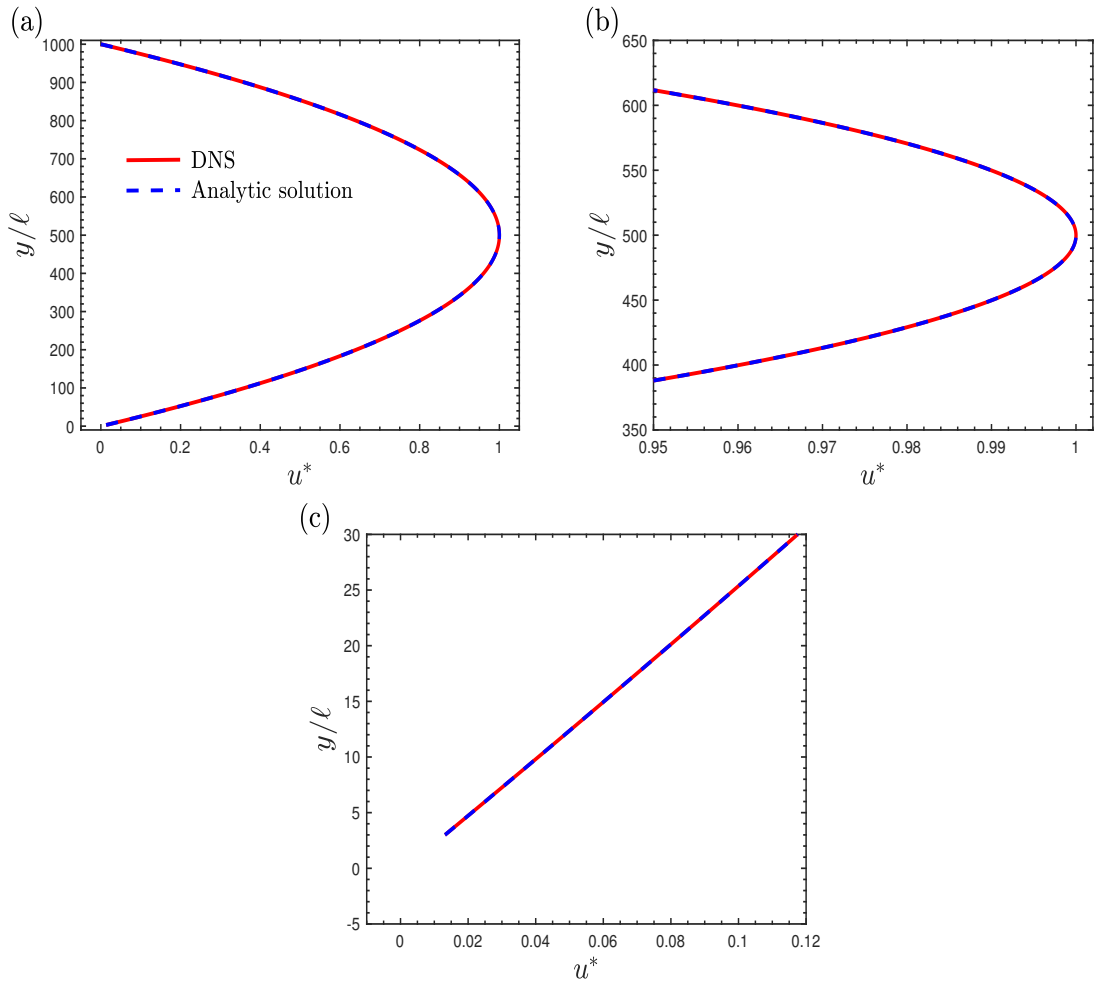


Fig. 12. Comparison of the local velocity profile in the free fluid obtained from the DNS at the cut line $x = 0$ with the predicted by Eq. (29) for $d_\eta = 3\ell$ and $u_\eta = 0.0165$. Local velocity profiles in (a) the whole undisturbed free flow domain, (b) around the maximum velocity neighborhood, and (c) the vicinity of $y = d_\eta$. The DNS is for the porous medium formed by cylinders in line with $C = 10^{-5}$, $L_\eta = 10^3\ell$, $L_\omega = 10^2\ell$, and $\varepsilon_{\beta\omega} = 0.8$.

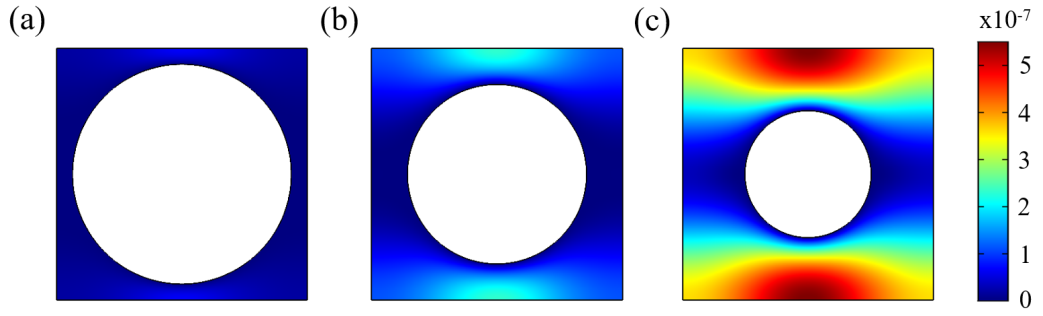


Fig. 13. Magnitude of the dimensionless local velocity in a unit cell of the bulk porous medium with a cylindrical particle for $C = 10^{-5}$ and three values of $\varepsilon_{\beta\omega}$: (a) 0.4, (b) 0.6, and (c) 0.8.

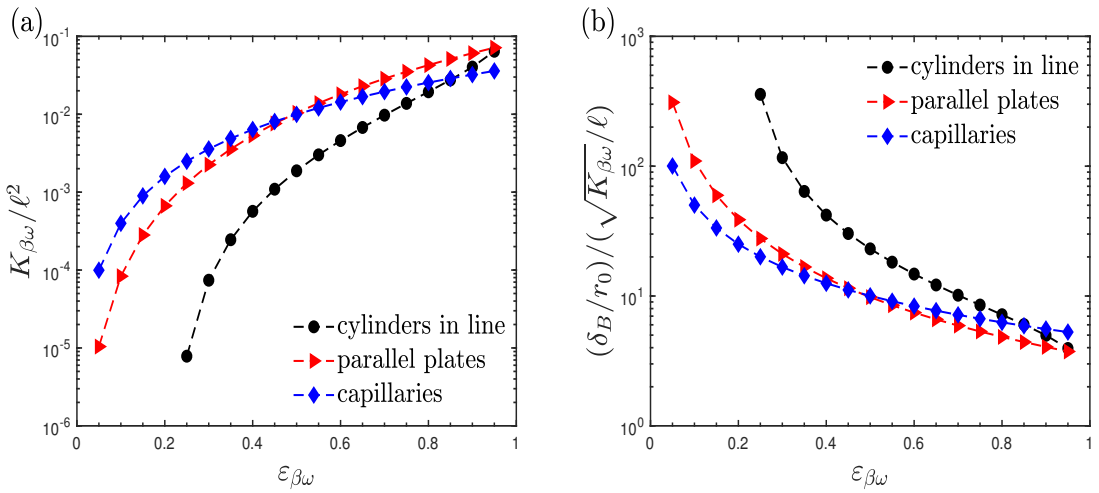


Fig. 14. Effect of $\varepsilon_{\beta\omega}$ on (a) the permeability of the bulk of the porous medium and (b) the ratio of the thickness of the Brinkman boundary layer to the square root of the porous medium bulk permeability.

In Fig. 14a we plot the dimensionless permeability as a function of $\varepsilon_{\beta\omega}$. As expected, the permeability is an increasing function of $\varepsilon_{\beta\omega}$. On the other hand, the ratio $\frac{\delta_B/r_0}{\sqrt{K_{\beta\omega}}/\ell}$ is shown in Fig. 14b. In addition, in figs. 14a and b, we also plot those results obtained for the two stratified porous medium configurations that were considered for the results shown in Fig. 8. Then, given the good agreement between the results for the inter-region of the two kinds of porous medium, it is possible to say that the porous medium permeability or configuration does not play a crucial role in the prediction of the average velocity profile. However, we can conclude that the size of the Brinkman boundary layer is much larger than the square root of the permeability of the bulk of the porous medium.

## 4 Discussion

In Sec. *2.3*, the limits of the applicability of Stokes model, for the flow in an analogous system to the channel that was used by Beavers and Joseph (1967), have been addressed . The results in this paper confirm for the first time that, even if a non-inertial formulation can be used to model the flow in the bulk of the homogeneous regions, in some cases it is necessary to include the inertial terms in the inter-region as it was done in the derivation of jump conditions by Ochoa-Tapia and Whitaker (1998). Our intention, in a further study, is to use the average velocity profiles obtained in the present paper to test the average

velocity equation resulting from upscaling the Stokes local flow problem. For that reason, we limited the DNS to the dimensionless pressure drop $C = 10^{-5}$.
In Fig. 7, it is clearly shown that there is a transition zone between the average velocity for samples located in the bulk of the fluid and the ones in the bulk of the porous medium where Darcy's velocity is reached. A rapid look at the velocity profiles that are shown in Fig. 7c suggests that the size of the transition zone ($\delta_B$) is the same than one half of the height of the averaging volume, $r_0$. This confirms the results previously reported by Ochoa-Tapia et al. (2017); those authors obtained the same type of behavior for the average velocity profile using as porous medium model one formed by capillary tubes parallel to the flow in the upper larger channel.

It should be noted that, even for a simplified representation of the particulate porous medium, the direct numerical simulations may be a very complicated approach if hundreds or thousands of unit cells are used to build some porous medium system of interest (*i.e.*, that satisfies certain characteristic length constrains). Then, other more practical alternatives that allow obtaining the average velocity profiles are appealling. For example, the expressions derived assuming capillary porous media by Ochoa-Tapia et al. (2017), or the ones presented in Appendix A of this paper for stratified porous media with pores formed by parallel plates. In this case, the local velocity profile between each two parallel plates is given by the well know Poiseuille model. Then, using an averaging operator, we could obtain analytical expressions for the average velocity profiles. Remarkably, the difference between the average velocity profile for the channel system with the stratified porous medium (*i.e.*, made of parallel plates or capilars) with that where the porous medium is made of cylindrical particles is not noticeable. This observation is maintained for different sizes of the averaging domain as long as $\varepsilon_{\beta\omega}$ is the same. The agreement is almost perfect also in the inter-region, as it is shown in Fig. 8. As mentioned earlier, the stratified plates or capillary geometry do not allow the mass and momentum transfer between both regions, such as in the geometry considered in the work of Ochoa-Tapia et al. (2017). However, this fact, either the porous medium configuration is granular or stratified, even that $\langle u_x \rangle_\omega^\beta$ is different (see Table 4), does not cause any significant difference between the average predicted velocity profiles in the inter-region. Again, the same comment can be said for any size of the averaging volume and $\varepsilon_{\beta\omega}$ value.

In the free flow part the average velocity profiles for different $\varepsilon_{\beta\omega}$ are essentially the same. The significant differences are located in the free flow/porous medium inter-region, as it is shown in Fig. 9. However, the velocity profiles for all porous medium configurations perfectly overlap for the same $\varepsilon_{\beta\omega}$.

Even accepting the possibility of application of the average velocity expressions obtained for stratified porous media, in Sec. *3.1*, the impact of the communication between the fluid of free flow and the one in the granular porous medium regions was determined. This effect was evaluated in terms of how the flow in one region modifies the velocity patterns corresponding to the bulk of the adjacent region. This analysis refers to the local velocity, the results are thus independent of any averaging process. In general, the results in Fig. 11 show that the size of the reach distance of the free flow on the porous medium region is $d_\omega < 5\ell$, while for the porous medium on the free flow is $d_\eta < 3\ell$. In addition, it should be noted that, without any doubt in the case of the systems with stratified porous medium $d_\omega = d_\eta = 0$. For such reason, to consider the influence of the communication between the two regions, the type, of data shown in figs. 7b and e are now presented in semi log format in Fig. 15. In those figures, it can be observed that the size of the Brinkman boundary layer, $\delta_B$, for granular systems is approximately

$$\delta_B \approx r_0 + \ell \tag{31}$$

It is clear that the penetration effect on $\delta_B$ becomes negligible as $r_0$ gets larger. In addition, for stratified systems $\delta_B = r_0$. Both penetration distances, $d_\eta$ and $d_\omega$ can be used to explain some of the results already shown above. For example, the effect of the bulk volume fraction on the velocity profile is limited to the inter-region as is shown in Fig. 9, in the rest of the domain the corresponding velocity profile is independent of $\varepsilon_{\beta\omega}$ and the porous media microstructure. This can be better explained in terms of Eq. (29), from which the position where the maximum velocity in the system is located can be obtained as

$$Y_{max} = \frac{1}{2}\left(\frac{L_\eta}{\ell} + \frac{d_\eta}{\ell}\right) - 2\frac{u_\eta}{C}\left(\frac{L_\eta}{\ell} - \frac{d_\eta}{\ell}\right)^{-1} \tag{32}$$

This equation, given that the characteristic length ratio $L_\eta/\ell = 10^3$ that was used to obtain the solution of the local velocity problem and the results $d_\eta \approx 3\ell$ and $u_\eta \approx 0.02$, can be simplified to

$$Y_{max} \approx \frac{1}{2}\frac{L_\eta}{\ell} \tag{33}$$

Using this result in Eq. (29) and the disparity of characteristic lengths of the system, previously used, the maximum velocity with $C = 10^{-5}$ is

$$u_{max} \approx \frac{1}{8} C \left( \frac{L_\eta}{\ell} \right)^2 = 1.25 \tag{34}$$

that is the result obtained from the DNS for all $\varepsilon_{\beta\omega}$ values. The use of the parabolic velocity profile in part of the channel system can be quite relevant for the solution of the flow problem given by the local equations, (11). The numerical solution for the sub-domain, $d_\eta \leq y \leq L_\eta$ could be avoided.

In addition, the distances $d_\eta$ and $d_\omega$ can help to justify the order of magnitude estimation for $\langle u_x \rangle^\beta |_{y=0}$, given by

$$\frac{\langle u_x \rangle^\beta |_{y=0}}{u_{max}} \approx \frac{r_0}{L_\eta} \left( \frac{2}{1 + \varepsilon_{\beta\omega}} \right) \tag{35}$$

This because Eq. (7), that was obtained for stratified porous media formed by parallel plates, for samples corresponding to the position $y = 0$ (*i.e.*, right in middle of the fluid/porous medium inter-region), together with the corresponding expressions in Table A.1, reduces to

$$\frac{\langle u_x \rangle |_{y=0}}{u_{max}} = \frac{1}{2} \left[ 2 \frac{r_0}{L_\eta} \left( 1 - \frac{2}{3} \frac{r_0}{L_\eta} \right) + \varepsilon_{\beta\omega} \langle u_x \rangle_\omega^\beta \right] \tag{36}$$

This result is valid for any $r_0$ and it is the arithmetic average of the flow rate in the free flow and the porous medium contained in the sample. For other stratified porous media, for which $d_\eta = d_\omega = 0$, the same result is obtained (Ochoa-Tapia et al., 2017). The physical meaning of $\langle u_x \rangle^\beta |_{y=0}$ is the same for any type of free flow/porous medium inter-region. However, for granular porous media Eq. (36) is not correct due to the penetration effect of the fluid of one region on the other. The use of Eq. (6) to replace $\langle u_x \rangle_\omega^\beta$ in Eq. (36) yields

$$\frac{\langle u_x \rangle |_{y=0}}{u_{max}} = \frac{r_0}{L_\eta} \left( 1 - \frac{2}{3} \frac{r_0}{L_\eta} \right) + \frac{1}{3} \left( \frac{\ell}{L_\eta} \right)^2 \varepsilon_{\beta\omega}^3 \tag{37}$$

that on the basis of $\frac{\ell}{L_\eta} \ll 1$ reduces to

$$\frac{\langle u_x \rangle |_{y=0}}{u_{max}} \approx \mathbf{O} \left( \frac{r_0}{L_\eta} \right) \tag{38}$$

Finally, the volume fraction at $y = 0$, given by

$$\varepsilon_\beta (y = 0) = \left( \frac{1 + \varepsilon_{\beta\omega}}{2} \right) \tag{39}$$

leads to the previous estimation for $\langle u_x \rangle^\beta |_{y=0}$, Eq. (35). The values that yield this equation are almost the same that the reported in Table 4 for the two stratified porous media. Furthermore, they are of the same order than the corresponding to the granular microstructures. It should be noted that all values are very close to each other for $r_0 \geq 10\ell$. In other words, for these sample sizes the penetration effects become negligible.

The relashionship of the Brinkman layer magnitude and the permeability is shown in Fig. 14b. From these results, we observe that this ratio increases as the size of the averaging volume is increased and it decreases as the value of $\varepsilon_{\beta\omega}$ is increased. Notice that the Brinkman boundary layer magnitude is of the order of the square root of the permeability of the bulk of the porous medium only when $r_0 = 2\ell$. Therefore, we may conclude that, in general, the Brinkman boundary layer is several orders bigger than the square root of the permeability of the bulk of the porous medium. Similar results were found using a porous medium made of square prism and staggered cylindrical particles. In addition, the stratified porous medium formulas, derived by Ochoa-Tapia et al. (2017) and the ones in Appendix A, allows to obtain the following relationships that can be used for $\delta_B$ estimation

$$\frac{\delta_B / r_0}{\sqrt{K_{\beta\omega}} / \ell} = \frac{2\sqrt{2\pi}}{\varepsilon_{\beta\omega}} \quad \text{for capillary pores} \tag{40a}$$

$$\frac{\delta_B / r_0}{\sqrt{K_{\beta\omega}} / \ell} = \frac{2\sqrt{3}}{\varepsilon_{\beta\omega}^{1.5}} \quad \text{for parallel plates pores} \tag{40b}$$

Also, it should be noted that, the previous estimations reported by Ochoa-Tapia and Whitaker (1995a), $\delta_B = \mathbf{O}(50) \sqrt{K_{\beta\omega}}$ and Goyeau et al. (2003), $\delta_B = \mathbf{O}(30) \sqrt{K_{\beta\omega}}$ are in good agreement with the results presented in this paper only for the case in which $r_0 \approx \ell$.

## 5 Conclusions

In this work, we studied the momentum transport between a free fluid and a porous medium in a similar system to the one used by (Beavers and Joseph, 1967). Here we addressed the question about the existence or not of a smooth transition zone in the average velocity profiles near the porous medium boundaries.

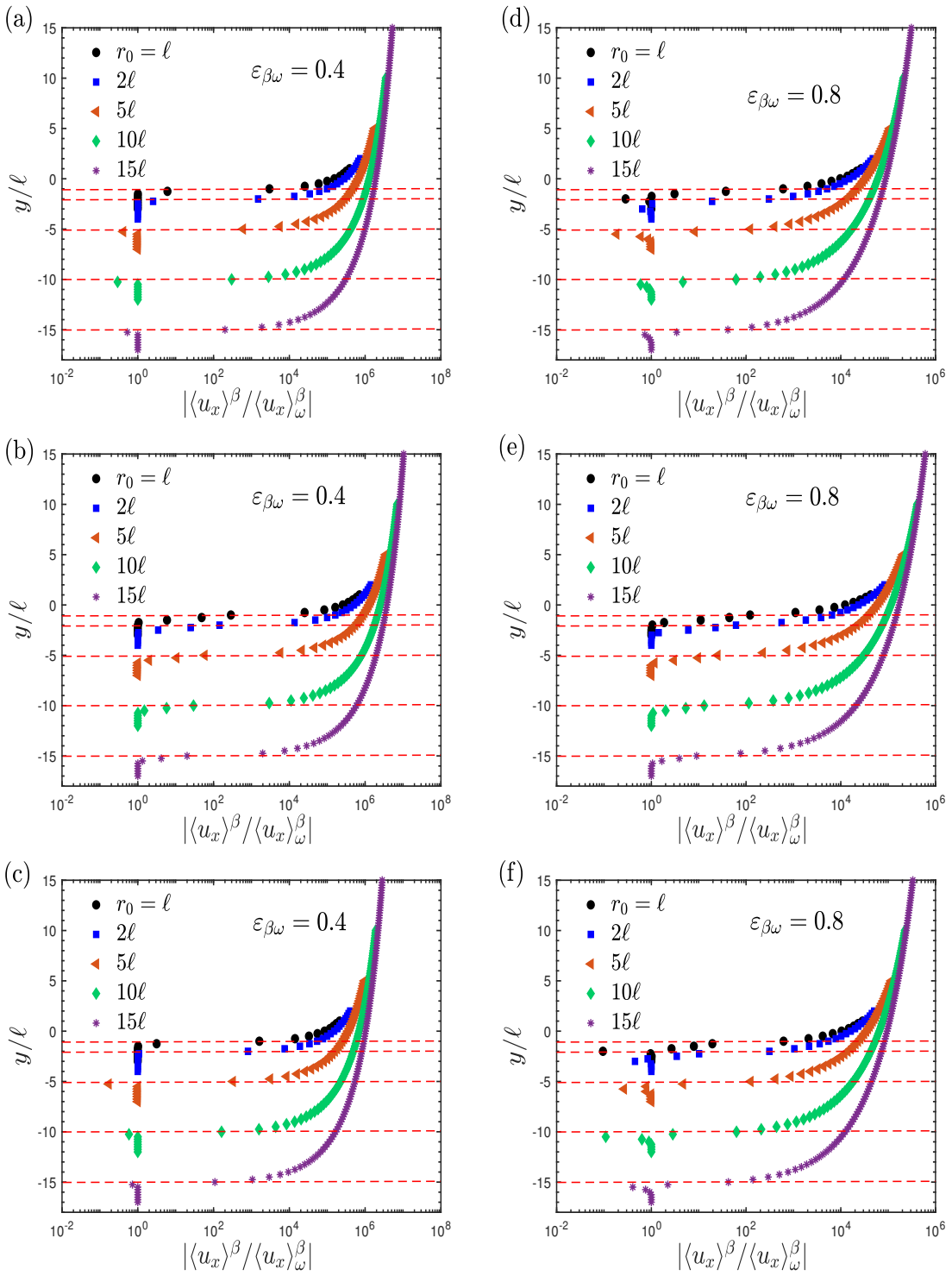


Fig. 15. Intrinsic average velocity profiles in the free fluid/porous medium inter-region as function of $\varepsilon_{\beta\omega}$ and the sample size, $r_0$. Porous medium microstructure: (a) and (d) cylinders in line, (b) and (e) staggered cylinders, and (c) and (f) square prisms in line. All DNS results are for $C = 10^{-5}$, $L_\eta = 10^3\ell$, and $L_\omega = 10^2\ell$.

From this analysis, we confirmed the existence of such smooth transition zone, although very small, in the average velocity profiles where the average velocity changes from the corresponding to samples fully located in the free fluid to the Darcy's velocity. Inside a porous medium, the size of this zone is almost one half of the height of the sample used for the averaging. This finding it is not a result of average transport equations obtained with some upscaling procedure as the averaging volume method or the homogeneization method. Therefore, in order to predict this transition zone, it may be neccesary to include additional terms in Darcy's law. This conclusion represents the major contribution of the present work and it completes the previous work of Ochoa-Tapia et al. (2017). In this sense, it was shown that for the flow in a channel system the communication between the flow in the free region and the one in the porous medium is not very important.

The results presented in this paper can be the benchmark for further study of the validity of average transport models in the inter-region and the careful deduction of jump boundary conditions. This type of information has not been published before.
Therefore, the analytical expressions of the average velocity profile provided in this work, and those presented in Ochoa-Tapia et al. (2017), acquire great importance, since they can reduce the computation time and they could be quite advantageous for further studies of heat and mass transfer between a free fluid and a porous medium.

## *Acknowledgments*

This work was benefited from Fondo Sectorial de Investigación para la educación from CONACyT (Project number: 256231). In addition, RHR (711177) expresses his gratitude to CONACyT for the economical support bestowed to carry out his doctoral studies.

## *Nomenclature*

| | |
|---|---|
| $\mathscr{A}_{\beta\sigma}$ | interfacial area inside of the porous medium |
| $C$ | dimensionless magnitude of the macroscopic pressure drop |
| $d$ | particle diameter, m |
| $d_j$ | distance of effect of $j-$region on the other ($j = \eta, \omega$), m |
| $f(y)$ | fraction of a pore contained in the averaging domain |
| $f_\beta(y)$ | fraction of the $\beta-$phase contained in $f$ |
| $\mathbf{g}$ | gravity vector, m$^2$ s$^{-1}$ |
| $\mathbf{K}_{\beta\omega}$ | permeability tensor of the bulk of the $\omega-$region, m$^2$ |
| $K_{\beta\omega}$ | tangential component of the permeability of the $\omega-$region, m$^2$ |
| $L_j$ | characteristic length of the $j-$region ($j = \eta, \omega$), m |
| $\ell$ | characteristic size of a unit cell that compose the $\omega-$region, m |
| $\ell_j$ | characteristic size of each phase in a unit cell that composes the $\omega$-region ($j = \beta, \sigma$), m |
| $m_\beta(\mathbf{r})$ | phase indicator function |
| $n_p(y)$ | number of pores contained in the averaging domain |
| $\mathbf{n}_{\beta\sigma}$ | unit normal vector from the $\beta-$phase towards the $\sigma$-phase |
| $\mathbf{n}_\beta$ | outwardly unit vector of the $\beta-$phase. |
| $p$ | dimensionless local pressure of the $\beta-$phase |
| $p_\beta$ | local pressure of the $\beta-$phase, N m$^{-2}$ |
| $p_{ref}$ | reference pressure, N m$^{-2}$ |
| $\tilde{p}_\beta$ | spatial deviation of the pressure of the $\beta-$phase, N m$^{-2}$ |
| $\mathbf{r}$ | position vector, m |
| $r_0$ | characteristic length of the averaging domain, m |
| $\mathrm{Re}_\eta$ | Reynolds number of the $\eta-$region. |
| $\mathrm{Re}_{p\omega}$ | Particle Reynolds number of the $\omega-$region. |
| $\mathbf{u}$ | dimensionless local velocity vector of the $\beta-$phase |
| $u_x$ | dimensionless horizontal component of the local velocity vector of the $\beta-$phase |
| $u_{max}$ | maximum velocity of the horizontal component of the intrinsic average velocity |
| $\mathbf{v}_\beta$ | local velocity vector of the $\beta-$phase, m s$^{-1}$ |
| $v_{\beta,x}$ | horizontal component of the local velocity vector of the $\beta-$phase, m s$^{-1}$ |
| $v_{ref}$ | reference velocity, m s$^{-1}$ |
| $v^j_{\beta x}$ | horizontal component of the local velocity of the $\beta-$phase in the $j-$region ($j = f, p$), m s$^{-1}$ |
| $v^j_{\max}$ | maximum local velocity in the $j-$region ($j = \eta, \omega$), m s$^{-1}$ |

| | |
|---|---|
| $\hat{v}_{\beta x}$ | line average of the horizontal component of the local velocity, m $s^{-1}$ |
| $\langle\varphi_\beta\rangle$ | superficial average of an arbitrary function associated to the $\beta-$phase |
| $\langle\varphi_\beta\rangle^\beta$ | intrinsic average of an arbitrary function associated to the $\beta-$phase |
| $\langle\varphi_\beta\rangle_j$ | superficial average of an arbitrary function associated to the $\beta-$phase in the $j-$region ($j = \eta, \omega$) |
| $V$ | volume of the averaging domain, $m^3$ |
| $V_\beta$ | volume of the $\beta-$phase contained in the averaging volume, $m^3$ |
| $\mathscr{V}$ | averaging volume |
| $\mathbf{x}$ | position vector locating the centroid of the averaging volume, m |
| $x$ | horizontal coordinate, m |
| $X$ | dimensionless horizontal coordinate |
| $\mathbf{y}_\beta$ | position vector relative to the centroid locating the $\beta-$phase contained in the averaging volume, m |
| $y$ | vertical coordinate, m |
| $Y$ | dimensionless vertical coordinate |

*Greek symbols*

| | |
|---|---|
| $\alpha_{BJ}$ | slip coefficient of the Beavers and Joseph's boundary condition |
| $\beta_{OTW}$ | stress jump coefficient of the Ochoa-Tapia and Whitaker boundary condition |
| $\delta_B$ | Thickness of the Brinkman boundary layer, m |
| $\mu_\beta$ | dynamic viscosity of the $\beta-$phase, N s $m^{-2}$ |
| $\mu_{eff}$ | effective viscosity, N s $m^{-2}$ |
| $\rho_\beta$ | density of the $\beta-$phase, kg $m^{-3}$ |
| $\varepsilon_\beta$ | volume fraction of the $\beta-$phase in any place of the system |
| $\varepsilon_{\beta\omega}$ | volume fraction of the $\beta-$phase in the $\omega-$region |
| $\varphi_\beta$ | arbitrary function associated to the $\beta-$phase |

## References


Angot, P., Goyeau, B., and Ochoa-Tapia, J. A. (2017). Asymptotic modeling of transport phenomena at the interface between a fluid and a porous layer: Jump conditions. *Physical Review E 95*, 063302.

Beavers, G. S. and Joseph, D. D. (1967). Boundary conditions at a naturally permeable wall. *Journal of fluid mechanics 30*, 197–207.

Beavers, G. S., Sparrow, E. M., and Magnuson, R. A. (1970). Experiments on coupled parallel flows in a channel and a bounding porous medium. *Journal of Basic Engineering 92*, 843–848.

Bird, R. B., Lightfoot, E. N., and Stewart, W. (2002). *Transport Phenomena*. Wiley.

Boudreau, B. and Jorgensen, B. (2001). *The Benthic Boundary Layer: Transport Processes and Biogeochemistry*. Oxford University Press.

Brinkman, H. (1949a). A calculation of the viscous force exerted by a flowing fluid on a dense swarm of particles. *Flow, Turbulence and Combustion 1*, 27.

Brinkman, H. (1949b). On the permeability of media consisting of closely packed porous particles. *Flow, Turbulence and Combustion 1*, 81.

Chandesris, M. and Jamet, D. (2006). Boundary conditions at a planar fluid–porous interface for a poiseuille flow. *International Journal of Heat and Mass Transfer 49*, 2137–2150.

Chandesris, M. and Jamet, D. (2007). Boundary conditions at a fluid–porous interface: an *a priori* estimation of the stress jump coefficients. *International Journal of Heat and Mass Transfer 50*, 3422–3436.

Clark, T. L., Mitchell, S. J., and Novak, M. (2007). Three-dimensional simulations and wind-tunnel experiments on airflow over isolated forest stands. *Boundary-layer Meteorology 125*, 487–503.

Eidsath, A., Carbonell, R., Whitaker, S., and Herrmann, L. (1983). Dispersion in pulsed systems III: Comparison between theory and experiments for packed beds. *Chemical Engineering Science 38*, 1803–1816.

Froment, G., Bischoff, K., and De Wilde, J. (2010). *Chemical Reactor Analysis and Design*. Wiley.

Goharzadeh, A., Khalili, A., and Jørgensen, B. B. (2005). Transition layer thickness at a fluid-porous interface. *Physics of Fluids 17*, 057102.

Goyeau, B., Lhuillier, D., Gobin, D., and Velarde, M. (2003). Momentum transport at a fluid–porous interface. *International Journal of Heat and Mass Transfer 46*, 4071–4081.

Jørgensen, B. (2001). Life in the diffusive boundary layer. *The Benthic Boundary Layer*. Oxford University Press, New York, NY, pages 348–373.

Macdonald, R. (2000). Modelling the mean velocity profile in the urban canopy layer. *Boundary-Layer Meteorology 97*, 25–45.

Margerit, J. and Séro-Guillaume, O. (2002). Modelling forest fires. part II: Reduction to two-dimensional models and simulation of propagation. *International Journal of Heat and Mass Transfer 45*, 1723–1737.

Morad, M. R. and Khalili, A. (2009). Transition layer thickness in a fluid-porous medium of multi-sized spherical beads. *Experiments in Fluids 46*, 323.

Neale, G. and Nader, W. (1974). Practical significance of Brinkman's extension of Darcy's law: coupled parallel flows within a channel and a bounding porous medium. *The Canadian Journal of Chemical Engineering 52*, 475–478.

Ochoa-Tapia, J. A., Valdés-Parada, F. J., Goyeau, B., and Lasseux, D. (2017). Fluid motion in the fluid/porous medium inter-region. *Revista Mexicana de Ingeniería Química 16*, 923–938.

Ochoa-Tapia, J. A. and Whitaker, S. (1995a). Momentum transfer at the boundary between a porous medium and a homogeneous fluid -I. Theoretical development. *International Journal of Heat and Mass Transfer 38*, 2635–2646.

Ochoa-Tapia, J. A. and Whitaker, S. (1995b). Momentum transfer at the boundary between a porous medium and a homogeneous fluid-II. Comparison with experiment. *International Journal of Heat and Mass Transfer 38*, 2647–2655.

Ochoa-Tapia, J. A. and Whitaker, S. (1998). Momentum jump condition at the boundary between a porous medium and a homogeneous fluid: inertial effects. *Journal of Porous Media 1*, 201–217.

Richardson, S. (1971). A model for the boundary condition of a porous material. part 2. *Journal of Fluid Mechanics 49*, 327–336.

Sahraoui, M. and Kaviany, M. (1992). Slip and no-slip velocity boundary conditions at interface of porous, plain media. *International Journal of Heat and Mass Transfer 35*, 927–943.

Seader, J., Henley, E., and Roper, D. K. (2016). *Separation Process Principles with Applications Using Process Simulators*, 4th Edition. Wiley.

Séro-Guillaume, O. and Margerit, J. (2002). Modelling forest fires. part I: A complete set of equations derived by extended irreversible thermodynamics. *International Journal of Heat and Mass Transfer 45*, 1705–1722.

Shavit, U. et al. (2009). Transport phenomena at the interface between fluid and porous domains. *Transport in Porous Media 78*, 324–540.

Taylor, G. (1971). A model for the boundary condition of a porous material. part 1. *Journal of Fluid Mechanics 49*, 319–326.

Valdés-Parada, F. J., Aguilar-Madera, C. G., Ochoa-Tapia, J. A., and Goyeau, B. (2013). Velocity and stress jump conditions between a porous medium and a fluid. *Advances in Water Resources 62*, 327–339.

Valdés-Parada, F. J., Alvarez-Ramírez, J., Goyeau, B., and Ochoa-Tapia, J. A. (2009). Computation of jump coefficients for momentum transfer between a porous medium and a fluid using a closed generalized transfer equation. *Transport in porous media 78*, 439–457.

Valdés-Parada, F. J., Goyeau, B., and Ochoa-Tapia, J. A. (2007). Jump momentum boundary condition at a fluid–porous dividing surface: derivation of the closure problem. *Chemical Engineering Science 62*, 4025–4039.

Whitaker, S. (1999). *The Method of Volume Averaging*. Kluwer Academic Publishers.

Yu, P. (2012). Numerical simulation on oxygen transfer in a porous scaffold for animal cell culture. *International Journal of Heat and Mass Transfer 55*, 4043–4052.

## Appendix A: Flow in a channel partially filled with a porous medium consisting of parallel plates

The objective of this appendix is to provide algebraic expressions for the average velocity profile in a

system like the one originally used by Beavers and Joseph (1967) and shown in Fig. 1. The simplicity of the formulas is possible due to the porous medium microstructure that is considered for the derivation. In this case, it is assumed that all the saturated pores are identical and formed by the space between two parallel rigid plates ($\sigma$-phase) separated a distance $2b = \ell_\beta$; the thickness of the solid plates is $\ell_\sigma$. In this way, the fluid volume fraction of the homogeneous porous medium is $\varepsilon_{\beta\omega} = 2b/\ell$, where $\ell = \ell_\beta + \ell_\sigma$, is the height of the unit cell. The free flow motion is through the gap, with separation $L_\eta = 2B$, formed by the surface of the last $\sigma$-phase plate and the upper wall of the channel. The details of the porous medium and samples in different zones of the system are shown in Fig. A.1. The procedure, to obtain the reported results, is essentially the one followed by Ochoa-Tapia et al. (2017) to obtain analogous expressions for a channel system with a porous media formed by identical cylindrical pores. It is worth remarking that the lack of communication among the fluid in the pores or fluid in the porous media and the free fluid may rise some doubt on the velocity profile predicted.

It is important to stress that, using this configuration, the flow in the $\eta$−region and in each pore are only connected at the entrances and exits of the channel. As a consequence, under the fully developed and unidirectional flow assumptions, the local velocity profile in the $\eta$−region is parabolic, with maximum velocity, $v^f_{max}$, given by

$$v^f_{max} = -\frac{dp_\beta}{dx}\frac{B^2}{2\mu_\beta} \tag{A.1}$$

Analogously, the local velocity profile in each pore is also parabolic where the maximun velocity of each pore is related to $v^f_{max}$ by

$$v^p_{max} = v^f_{max}\left(\frac{b}{B}\right)^2 \tag{A.2}$$

## *A.1 Average velocity profiles*

Due to the fully developed flow assumption, the equation to obtain the superficial volume average velocity, Eq. (2a), is simplified to

$$\langle v_\beta \rangle = \frac{1}{2r_0}\int_{\zeta=y-r_0}^{\zeta=y+r_0} m_\beta(\zeta)v_\beta(\zeta)d\zeta \tag{A.3}$$

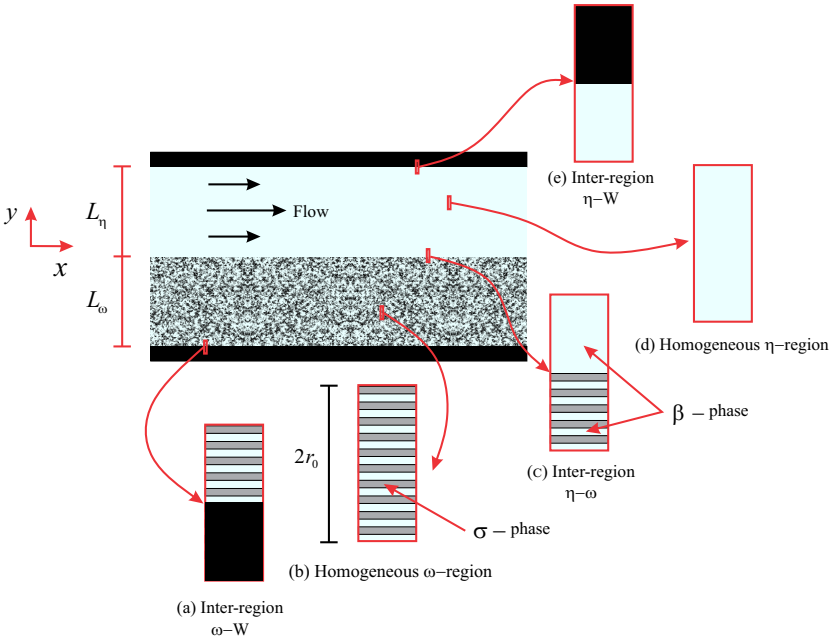


Fig. A.1. Channel partially filled with a porous medium made of an array of parallel plates and samples in both homogeneous regions and the inter-regions.

where $y$, indicates the position of the centroid of the sample and the hight of the sample volume is $2r_0$. The origin of the vertical coordinate $y$ is located at the upper boundary of the porous medium. In the following paragraphs, the average velocity formulas for each one of the five characteristic zones of the system are presented.

## *A.2 Zones that do not depend on the microstructure of the porous medium*

### *A.2.1 Free fluid/upper wall inter-region ($\eta W-$ inter-region)*

In this zone the averaging volume contains portions of free fluid and upper wall. Application of Eq. (2a) yields

$$\frac{\left\langle v_\beta \right\rangle_{\eta W}}{v^f_{\max}} = \frac{B}{2r_0}\left[\frac{2}{3} - \frac{y-B-r_0}{B} + \frac{1}{3}\left(\frac{y-B-r_0}{B}\right)^3\right], \quad \text{for } L_\eta - r_0 \le y \le L_\eta + r_0 \tag{4}$$

Here it should be noted that, $\left\langle v_\beta \right\rangle_{\eta W} = 0$ at $y = L_\eta + r_0$. In this position, the averaging volume is located completely inside the impermeable wall. Thus the average velocity is equal to zero in $y = L_\eta$ only if $r_0 \ll B$.

### *A.2.2 Homogeneous free fluid (homogeneous $\eta-$region)*

In this zone, that it is also independent of the porous medium, all averaging volumes are fully located in the free fluid, the average velocity is given by

$$\frac{\left\langle v_\beta \right\rangle_{\eta}}{v^f_{\max}} = \left[1 - \frac{1}{3}\left(\frac{r_0}{B}\right)^2 - \left(\frac{y}{B} - 1\right)^2\right], \quad \text{for } r_0 \le y \le 2B - r_0 \tag{5}$$

It should be noted that this expression is reduced to the local velocity equation, provided that the size of the averaging region is much less than the separation gap of the upper channel, *i.e.*, $r_0 \ll B$.

## *A.3 Zones that depend on the microestructure of the porous medium*

### *A.3.1 Homogeneous porous medium region (homogeneous $\omega-$region)*

In this zone, where the samples are fully located in the porous medium, the superficial average velocity Darcy's velocity is given by

$$\langle v_\beta \rangle_\omega = v^p_{max}\frac{2}{3}\varepsilon_{\beta\omega} = v^p_{max}\frac{4}{3}\frac{b}{\ell} = v^f_{max}\frac{4}{3}\frac{b}{\ell}\left(\frac{b}{B}\right)^2, \quad \text{for } -L_\omega + r_0 \le y \le -r_0 \tag{6}$$

Here, it has been used that, the fluid volume fraction in the homogeneous porous region is $\varepsilon_{\beta\omega} = \frac{2b}{\ell}$.

### *A.3.2 Inter-regions that contain porous medium*

The inter-regions that contain porous medium are two: one between the porous medium and the free fluid and the other between the porous medium and the lower wall of the channel. The average velocity in both cases can be represented by

$$\left\langle v_\beta \right\rangle_{\omega\lambda} = \frac{1}{2r_0}\left[(y + r_0)\,\bar{v}^{f,\omega\lambda}_\beta + n_p \ell_\beta \left\langle v_\beta \right\rangle^\beta_\omega + f_\beta \ell \bar{v}^{p,\omega\lambda}_\beta\right], \quad \lambda = \eta, W \tag{7}$$

where, from eqs. (6) and (A.2), $\langle v_\beta \rangle^\beta_\omega = \varepsilon_{\beta\omega}\langle v_\beta \rangle_\omega$. The contributions $(y + r_0)\,\bar{v}^{f,\omega\lambda}_\beta$ and $f_\beta \ell \bar{v}^{p,\omega\lambda}_\beta$, for $\lambda = \eta$ or $W$, are reported in Table A.1.

It should be noted that, unlike the $\eta\omega-$ inter-region, in Eq. (7) there is not a contribution of the free fluid. Furthermore, the average velocity is null at $y = -L_\omega - r_0$. Namely, when the averaging volume is located totally within the lower impermeable wall. Details of the derivations presented in this section are reported by Hernandez-Rodriguez (2018).

Note that, to obtain the dimensionless average velocity profile, $\left\langle v_\beta \right\rangle / v^f_{max}$ as funtion of $y/\ell$, it is necessary to fix $\varepsilon_{\beta\omega}, L_\eta$, $L_\omega$ and $r_0/\ell$. In Fig. 9, the dimensionless average velocity profiles obtained with DNS are compared with the resulting from the formulas presented in this section.

Table A.1. Summary of the analytic expressions, of the contributions $(y + r_0)\,\bar{v}_\beta^{f,\omega\lambda}$ and $f_\beta \ell \bar{v}_\eta^{p,\omega\lambda}$, to evaluate the intrinsic average velocity profile in the inter-region, $\eta\omega$ or $\eta W$, with Eq. (7).

| Inter-region | $\omega\eta$ | $\omega W$ |
|---|---|---|
| $\lambda$ | $\eta$ | W |
| centroid position domain | $-r_0 \leq y \leq r_0$ | $-L_\omega - r_0 \leq y \leq -L_\omega + r_0$ |
| $\dfrac{(y + r_0)\,\bar{v}_\beta^{f,\omega\lambda}}{v_{\max}^f}$ | $\frac{(y+r_0)^2}{B}\left[1 - \frac{1}{3}\left(\frac{y}{B} + \frac{r_0}{B}\right)\right]$ | 0 |
| $\dfrac{f_\beta \ell \bar{v}_\beta^{p,\omega\lambda}}{v_{\max}^f \left(\frac{b}{B}\right)^2}$ | $\frac{\varepsilon_{\beta\omega}\ell}{2}\left[\frac{2}{3} - \frac{b - f_\beta\ell}{b}\left(1 - \frac{1}{3}\left(\frac{b-f_\beta\ell}{b}\right)^2\right)\right]$ | $\left(\frac{f_\beta\ell}{3b}\right)^2\left(3 - \frac{f_\beta\ell}{b}\right)$ |
| $n_p\,(y)$ | $\left\lfloor -\left(\frac{y-r_0}{\ell}\right)\right\rfloor$ | $\left\lfloor \frac{y+L_w+r_0}{\ell}\right\rfloor$ |
| $f\,(y)$ | $-\left(\frac{y-r_0}{\ell}\right) - n_p$ | $\frac{y+L_w+r_0}{\ell} - n_p$ |
| $f_\beta\,(y)$ | $0$, if $f \leq (1 - \varepsilon_{\beta\omega})$ | $f$, if $f < \varepsilon_{\beta\omega}$ |
| $f_\beta\,(y)$ | $f - (1 - \varepsilon_{\beta\omega})$, if $f > (1 - \varepsilon_{\beta\omega})$ | $\varepsilon_{\beta\omega}$, if $f < \varepsilon_{\beta\omega}$ |